Department of Physics and Astronomy
University of Heidelberg

Bachelor Thesis in Physics
submitted by

Vincent C. Mader

born in Ulm (Germany)

February 2020

Gas accretion onto eccentric planets

This Bachelor Thesis has been carried out by Vincent C. Mader at the
Max Planck Institute for Astronomy in Heidelberg
under the supervision of
Dr. Bertram Bitsch

Abstract

When trying to study the processes involved in planet formation utilizing algorithms of computational fluid dynamics, it is often necessary to explicitly specify a model for the accretion rate of gas onto a planet. Various methods for this exist, but often it is assumed that the accretion rate can be calculated without taking the planet's orbit eccentricity into account.

In this thesis, a simplified model of a proto-planetary disk is created using the *FARGO2D1D* algorithm, with which studies of various disk and planet parameters are made. The goal of this work is to show that the orbit eccentricity can play a large role in the accretion rates of disk material onto a planet. This is due to the fact that planets on highly eccentric orbits form much broader gaps in the disk via the exchange of angular momentum than would be the case for a planet on a circular orbit. These gaps are accordingly more shallow, leading to a higher gas density in the planet's Hill sphere and therefore faster accretion.

If one tries to create an accurate model of the accretion processes occurring inside proto-planetary disks, it might be advantageous to take the orbit eccentricity into account when formulating an accretion routine, especially when studying systems around very young stars, where eccentricities on average are still much higher than they are in our own Solar System today.

Zusammenfassung

TODO: translate from above

Acknowledgements

I wish to express my deepest gratitude to Dr. Bertram Bitsch for giving me the opportunity of writing my bachelor's thesis under his supervision at the Max Planck Institute for Astronomy, and am very grateful to him for always being available with helpful answers to the questions and problems facing me during the writing of this work.

I want to thank Camille Bergez-Casalou as well, who quite a few times helped me out with friendly advice when it came to the intricaties of the FARGO2D1D code or the usage of the computer cluster.

Also, I am very grateful to Prof. Kees Dullemond for taking on the task of acting as second proof-reader, as well as Dr. Coryn Bailer-Jones, for inspiring me during a seminar to write my bachelor's thesis at the MPIA and for helping me establish contact with Bertram. In general, I wish to express my gratitude to Ruperto Carola University and to the MPIA Heidelberg, for the knowledge and opportunities they granted me.

Lastly, I wish to thank my mother for making it possible for me to study physics in Heidelberg, as well as my grandmother, who from an early age on inspired me to think critically and to remain curious about the universe.

Contents

List of Figures

List of Tables

Chapter 1

Introduction

1.1   Historical Context

As early as the time of the ancient Babylonian civilization, several bright objects could be distinguished from the rest of the the night sky. In contrast to the stars, which on human timescales constitute a relatively static background, these objects seemed to exhibit independent motion across the sky. This explains why the word we use today to describe these objects is *planet*, which has its origin in the ancient Greek *planetes*, literally meaning "wanderer". It was observed that every now and then, the movement of these sources of light seemed to stop and then reverse for a while. Nowadays, we of course know that this behavior is explained by the planets' independent motion around the Sun. Although it was suggested that the Earth does not make up the center of the universe relatively early, e.g. by Aristarchus of Samos in the third century B.C.E., this was not a widely accepted fact until relatively recent times.

Up until the Renaissance, the widespread world view followed a model most notably suggested by the Greek polymath Ptolemy, who argued for a geocentric universe, where the Sun, planets and stars all orbit the Earth. Each of the orbiting planets was thought to additionally travel on a so-called epicycle, which helped explain the fact that the observed planets did not always travel in the same direction in the sky as seen from Earth.

Due to their low apparent magnitudes, the planets Mercury, Venus, Mars, Jupiter and Saturn can be observed from Earth with the naked eye. Thus, they were known to most historic societies with any interest in astronomy. Not being able to explain their origin, humans in civilizations all over the world tried to give these mysterious sources of light meaning by incorporating them into their stories, mythologies and religions.

It would take almost two millenia before the heliocentric model of the solar system gained widespread attention. In the 16th century, the Polish polymath Nicolaus Copernicus formulated a model of the universe with the Sun at its center and the planets traveling around it on concentric circles. Eventually, the observations of Mars' orbit done by Johannes Kepler and his mentor Tycho Brahe lead to the a new empirical description of the motions of astronomical bodies that improved on the model of Copernicus, known to us today as Kepler's laws. Among other things, Kepler realized that the planets move around the sun not on circles, but on ellipses, with the Sun positioned at one of the foci.

These observations would lead Isaac Newton to formulate his theory of gravity together with his laws of motion which, it could be argued, marked the start of the scientific revolution that would take place in the following centuries. He regognized that a simple inverse square law suffices to predict the motions of the astronomical bodies in a relatively accurate way. Additionally, he noticed that this same law held true not only for the planets, but also for any falling object here on Earth.

The new heliocentric world view provided a lot of new questions in need of answers during the following centuries. Are all stars actually suns like our own, only much farther away? Could there be planets orbiting those stars and could those planets look like our own home planet, possibly even with their own unique life forms and evolutionary histories?

An attempt to explain the origin of the Solar System was made in the 18th century in part by Immanuel Kant and Pierre-Simon Laplace in their *nebular hypothesis*, in which they argued for the former existence of a giant gas cloud. Slowly rotating, this cloud was suspected to have collapsed and subsequently flattened out due to its own gravitaty. Later on, the Sun and the planets were thought to have emerged from the gas.

After the invention of the first (semi-)modern telescopes by Galileo and Newton, the following centuries saw the discoveries of more planets in our own solar system. First Uranus in the late 1700s, then Neptune a century later, bringing the number of known planets in our solary system to eight. The discovery of Pluto and later many other objects of the same size in the outer solar system prompted the *International Astronomical Union* to formally define the term *planet* in 2006 [**cite**]. For any object in the Solar System to be classified as a planet, it has to

1. be in direct orbit around the Sun
2. possess a mass large enough to assume a nearly round shape due to self-gravitation
3. have cleared its orbit of any larger or similarly-sized bodies

With continuing scientific and technological progress, telescope resolution improved drastically, increasing the observing distance of astronomical bodies. Larger and more accurate telescopes, as well as the eventual possibility of launching those telescopes into orbit made the discovery of extrasolar planets feasible. The first discovery of such an exoplanet was confirmed by Wolszczan and Frail (1992) with about 5000 having been observed since then, most notably by the *Kepler Space Telescope*, with which alone about 2600 planets could be detected. The first direct observation of a nascent proto-planet inside a proto-planetary disk was reported in 2018, after the exoplanet *PDS 70b* was imaged using ESO's *Very Large Telescope* (Keppler et al., 2018).

These recent observations show that planets are very abundant and that there might be more stars with an own planetary system than without [20]. Observations by e.g. Petigura, Howard, and Marcy (2013) indicate that a significant portion of stars is accompanied by Earth-sized planets inside the Goldilocks zone, where liquid water can exist in a stable form and therefore one of the basic requirements for life is fulfilled. Extrapolating from these observations, it is possible that there could up to 40 billion Earth-like planets in the Milky Way alone.

The mass of observed planets ranges from about twice that of the Moon to about 30 times that of Jupiter, thus spanning multiple orders of magnitude. Planetary compositions depend largely on their size. Most modern planetary formation theories assume an initial buildup of a central rocky core. From there the planet evolves either into an Earth-like terrestrial planet or into a gaseous giant similar to Jupiter (W. Kley et al., 1999).

The processes underlying planet formation are yet to be fully explained by science. Accurate modeling requires an understanding of many different aspects of the natural sciences, including but not limited to magneto-hydro-dynamics, chemistry, gravity (n-body-dynamics), thermodynamics, radiative transfer and coagulation physics. Due to temporal constraints and the complexity of the topic, this bachelor's thesis can only cover a small portion of what there is to be said about this active field of study.

1.2   Proto-Planetary Disks

The current scientific consensus on the origin theory of stars and planets is based on the nebular hypothesis, which states that proto-planetary disks form when large interstellar clouds of molecular gas collapse under their own gravity [22]. The chemical composition of these disks is dominated by the contribution of molecular H_2, which in most cases makes up about 98% of the disk by mass. Besides that, there are also small quantities of helium, lithium and trace amounts of heavier elements. In observed disks, most of the matter is present in the form of gas, but some of it also exists as dust. The exact ratio of dust to gas and the distribution of these two components throughout the disk is still largely unknown [4][24].

The collapse of such a cloud leads to a drastic increase of gas density, pressure and temperature at its center, which for high mass clouds results in the formation of a star. Conforming to the law of momentum conservation, the cloud's angular velocity increases during the collapse. Also, the initially present statistical distribution of velocities averages out in favor of the clouds's net angular momentum. The centrifugal force present in a rotating reference frame can only balance out the pull of gravity along the radial axis. Therefore, the cloud flattens out into a disk much more wide than thick, supported only by gas pressure along the axis orthogonal to the disk. Typical disk radii are on the order of a few 100 AU [23].

The flattened cloud can also be regarded as an accretion disk around the central star, which after an initial accretion phase makes up almost all ($> 99\%$) of the mass in the disk. Planets form from the remaining gas in orbit around the star. This gas heats up due to friction and radiates away energy, which can be observed with submillimeter telescopes. Figure 1.1 shows two images of proto-planetary disks that were observed at the *Atacama Large Millimeter/submillimeter Array* (ALMA). In them, multiple circular dark regions can be seen. Those are regions where the gas has partially been depleted by an exchange of angular momentum with the planet.
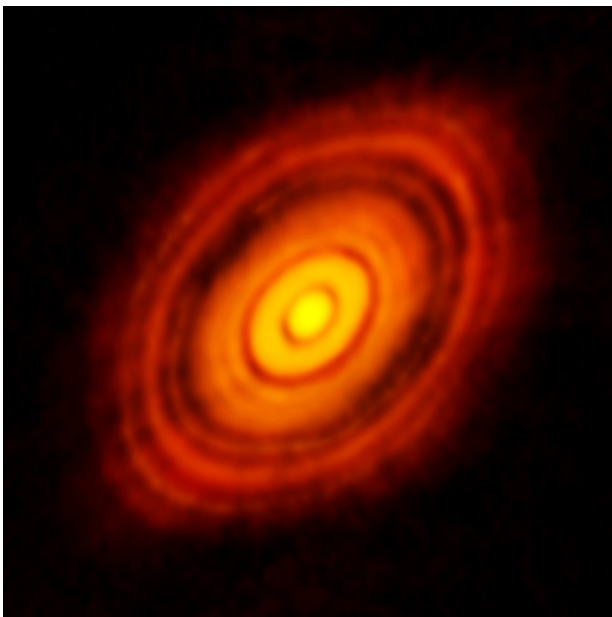
(a) Disk around *HL Tau* [1]   (b) Disk around *TW Hydrae* [2]
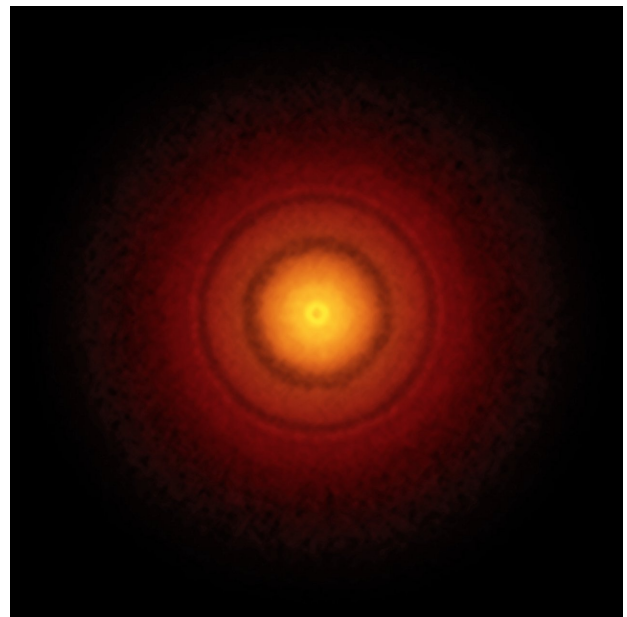
Figure 1.1: proto-planetary disks around the stars *HL Tau* and *TW Hydrae*, observed at submillimeter wavelengths at *ALMA*. The dark rings indicate regions of lower gas density, hinting at the existence of exoplanets.

To construct a simplified model of a proto-planetary disk in two dimensions, we use cylindrical coordinates (r, φ, z). In this model, the disk is situated at $z = 0$ and is infinitesimally thin. Since observations show proto-planetary disks to be much more wide than thick anyways, this assumption makes it possible to obtain a relatively accurate, yet much less computationally constraining model. It allows us to ignore the z-dependence of the parameters describing the disk, including gas density, temperature and rotational velocity. Going from a 3D model to a 2D model in this way naturally suggests the definition of a surface density

$$\Sigma(r, t) = \int_{-\infty}^{\infty} \rho(z, t) \cdot dz \tag{1.1}$$

In this highly simplified model, all inhomogenities in the chemical composition of the disk are neglected. The disk is assumed to consist entirely of individual gas particles with a mean molecular mass m_{mol} and uniform temperature T. If the gas were perfectly non-viscous, the trajectory of such a gas particle in the gravitational potential of a star with mass M_* would be described by Kepler's laws. Assuming a circular orbit, the angular frequency could then be expressed as

$$\Omega_K = \sqrt{\frac{GM_*}{r^3}} \tag{1.2}$$

In reality, the gas in a disk does not orbit its parent star in a perfectly Keplerian way, since the non-neglectable viscosity of the gas leads to slightly lower rotation velocities than one would expect from Equation 1.2. If, additionally, a planet is present in the disk and its interactions with the gas are taken into account, the trajectories of individual bodies (planet or gas particles) in this system become impossible to determine analytically, therefore making the utilization of numerical simulations very attractive.

Since they mostly probe the outer domains of proto-planetary disks, millimeter observations as of yet do not give much information about the gas density profile in the inner regions of the disk (Dullemond and Monnier, 2010). A first approach to modeling the gas surface density's dependency on r is be to assume a simple power law:

$$\Sigma(r) = \Sigma_0 \cdot \left(\frac{r}{r_0}\right)^{-\gamma} \tag{1.3}$$

In our case, r_0 labels the distance of the planet from the star and $\Sigma_0 := \Sigma(r_0)$ is the surface gas density at the position of the planet. The slope of $\Sigma(r)$ is characterized by the parameter γ, will is assumed to be $= 1$ in thesis.

Even though the disk will be treated as a 2D object in this thesis, it is important to talk about the geometry of real disks observed in the night sky. Contrary to what one might expect without any prerequisite knowledge, observations show that the spatial extension in z-direction of proto-planetary disks grows larger with increasing distance from the star. An approximation of this can be made by expressing the surface scale height H as a polynomial function of the distance from the center r. With $H_0 := H(r_0)$, this can be written as

$$H(r) = H_0 \cdot \left(\frac{r}{r_0}\right)^{\beta} \tag{1.4}$$

Here, β labels the so-called *flaring index*. A sketch of a non-flaring as well as a flaring disk can be seen in Figure 1.2.

Equation 1.4 suggests the definition of another useful parameter, namely the *aspect ratio*

$$h_r(r) := H(r)/r \tag{1.5}$$

A commonly used value to set up the disk's ratio of height to width is $h_r(r_0) = 0.05$ (see e.g. W. Kley et al., 1999), which will be used in most of the simulations discussed in this thesis.

To model the disk's viscosity, the α-description is used:

$$\nu = \alpha \frac{c_s^2}{\Omega_K} \tag{1.6}$$

It is assumed that the parameter α_{visc} is constant throughout the disk and does not change with time. Observations of real proto-planetary disk show typical values to be roughly around 0.1, whereas for numerical simulations the alpha parameter is often assumed to be a magnitude smaller and is commonly set to $\alpha_{visc} = 10^{-2}$ (e.g. Baillié, Charnoz, and Pantin, 2016). Reasons for this disrepancy have been described by King, Pringle, and Livio (2007). The viscous evolution of the gas surface density over time is taken from Lynden-Bell and Pringle (1974), where it is expressed as

$$\frac{\partial \Sigma}{\partial t}(r,t) = \frac{3}{r} \cdot \frac{\partial}{\partial r}\left(\sqrt{r} \cdot \frac{\partial}{\partial r} \nu \Sigma(r,t) \cdot \sqrt{r} \right) \tag{1.7}$$

Under the assumption of hydrostatic equilibrium, the disk's local isothermic sound velocity can be expressed as

$$c_s = H \cdot \Omega_K = h_r \cdot v_K \tag{1.8}$$

and the pressure of the gas is described by

$$P = c_s^2 \cdot a \cdot \Sigma \tag{1.9}$$

This last equation will be of importance when investigating the eccentricity of the gap that forms around the planet. For this, the gap boundaries need to be determined, which can be done by calculating the maxima and minima in the gas pressure gradient. (TODO: adjust the last few sentences since I probably won't be using the pressure gradient method)

(a) non-flaring disk   (b) flaring disk
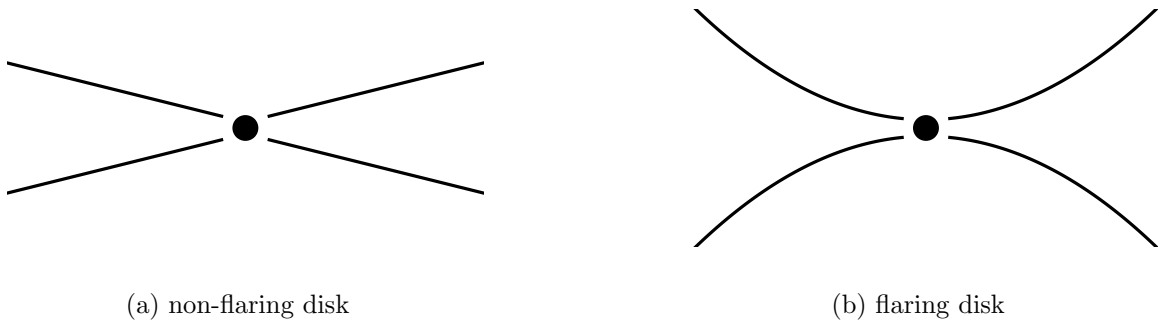
Figure 1.2: Qualitative sketches of the difference between flaring and non-flaring disks

1.3   Planets in the Disk

1.3.1   Formation

Most standard planet formation theories assume the initial buildup of a central rocky core [26]. From this point on, the proto-planet may either develop into a terrestrial planet or into a giant planet consisting of a rocky core and a large gaseous hull. In our own Solar System, the four terrestrial planets are those situated closest to the Sun, while the four gas giants sit in the outer regions of the Solar System.

This is probably no coincidence. Most of the matter in the universe, and therefore most likely also in newly formed disks, consists of light elements like hydrogen and helium. Because of the radiation pressure of the solar wind, these light elements accumulate in the outer regions of the disk. Therefore, an accreting planetoid in the outskirts of the disk has much more material available for accretion in its vicinity than one close to the center.

In the early stages of planet formation, gravity does not play a dominant role. Gas and dust grains collide and stick together mainly via microphysical processes like van der Waals or Coulomb forces [27]. These processes are not still entirely understood today . It is unclear how the early planet cores manage to grow without fragmenting into smaller pieces again at collisions with other, similarly-sized planetesimals. This problem is known as the meter-sized barrier [19].

The early development of planetesimals will not be studied in this thesis. It is assumed that the initial buildup of a planet core has already taken place. From this point on, planets grow either by direct collisions with other bodies or via gravitational capture (Morbidelli and Raymond, 2016). This leads to the eventual formation of circumplanetary accretion disks similar to the proto-planetary disk itself, but on much smaller scales.

The accreted material comes mostly from inside the planet's Hill sphere (also called the Roche sphere). This is the region in space where the gravitational influence of the planet's is larger than that of its central star [5]. If a body with mass m orbits a larger mass M with a semi-major axis a and eccentricity e, the radius of the Hill sphere can be approximated by

$$r_H \approx a(1-e)\sqrt[3]{\frac{m}{3M}} \qquad (1.10)$$

To simulate a proto-planetary disk, this thesis makes use of the *FARGO2D1D* algorithm, which will be discussed in detail in section section 2.1. The code makes use of both a Kley and Machida accretion subroutine, which are also given a detailed description in that section (mention other accretion mechanisms than Kley & Machida). For most simulations, the planet will be kept on a fixed orbit so that there is no migration.

1.3.2   Gap Formation

Recent observations of proto-planetary disks often show dark, circular regions around the star [1][2]. It is assumed that these are created by forming proto-planets orbiting the star. When sufficiently grown, a proto-planet exerts tidal torques on the disk and thereby induces trailing spiral shocks (Kley, 1999). Via these, angualar momentum is transfered between the disk and the planet, which has the effect of material being pushed away from the proto-planet. To be more precise, the planet loses some of its angular momentum to the outer part of the disk, while it receives some from the inner part.

This process eventually leads to the the opening of a gap in the disk. The detailed criteria for the gap opening process are discussed in detail in Lin & Papaloizou (1986, 1993) as well as Crida (2006). The width, i.e. extent in radial direction, of the gap depends on the mass of the planet, as well as the viscosity and gas pressure in the disk (Lin and Papaloizou, 1993).

After the formation of the gap, there is still accretion from regions outside or inside the planet's orbital radius, since the internal evolution of the disk tends to spread the gas back into the void regions by diffusion (W. Kley et al., 1999). Thus, the accretion rate after gap opening has occurred is further influenced by the thickness of the disk as well as the viscosity of the gas.

1.3.3   Migration

The interaction of the a growing proto-planet with the gas in the disk can lead to a change in the orbital parameters of the proto-planet, most importantly a change in the planet's semimajor axis, i.e. migration of the planet (Dürmann and Kley, 2015). Depending on the mass of the planet, different categories can be distinguished to describe the migration.

For low-mass planets not massive enough to open up a gap in the disk (less than about 50 Earth masses), type I migration occurs. The total torque acting on a planet is given by the sum of Lindblad torques and the corotation torques generated by the gas flow in the coorbital horseshoe region [7] [21]. We will not focus on type I migration since all planets in this thesis have masses on similar orders of magnitude as Jupiter.

For massive planets, type II migration occurs. Due to angular momentum deposition in the disk, a gap opens up in the disk. This gap will have to move through the disk with the planet. It is often assumed that in an equilibrium situation, the gap moves at exactly the same speed as the planet, and that the planet is locked in the middle of the gap to maintain torque equilibrium [7][16].

Chapter 2

Methods

2.1 The *FARGO2D1D* Algorithm

The *FARGO* algorithm was originally introduced by F. Masset (1999). The algorithm's name is an acronym for *Fast Advection in Rotating Gaseous Objects*. It is written in C and utilizes a 5th order *Runge-Kutta* subroutine to determine the trajectory of a planet in the disk, as well as a fluid dynamics subroutine for the gas. It is possible to configure whether the planet should interact only with its parent star or also with the gas in the disk, allowing for simulations of planet migration. The gas feels only the gravitational potential of the star. Accretion of gas onto the planet therefore has to be handled in a simplified way, which will be discussed over the next few paragraphs.

To model a protoplanetary disk, it is represented in the code simply by a 2D grid. Each grid cell stands for a specific location in the disk. The row and column of such a cell correspond to its radial and azimuthal position.

In this thesis, an extension of the standard version of *FARGO* is utilized, titled *FARGO2D1D*. Here, the 2D grid is surrounded by an additional, one-dimensional grid made of elementary rings. The planet is placed within the 2D section of the grid. Far from the center, the gravitational influence of the planet on the structure of the disk is diminishingly small [10]. Because of this, the disk can be assumed to be axisymmetric for large values of r.
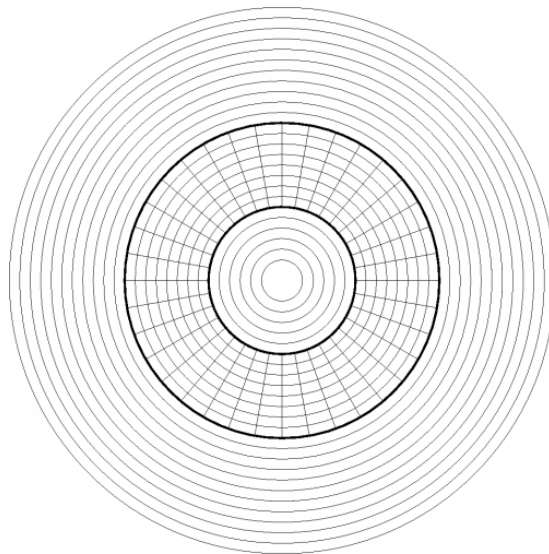
Figure 2.1: Sketch of the grid that is being used by the *FARGO2D1D* algorithm [9]. It consists of both a one-dimensional section and a two-dimensional section. In the latter, the planet is placed.

The algorithm in principle allows to have multiple planets in a single disk, all interacting with each other and with the disk. In this thesis though, only a single planet is inside the disk at any given time. At $t = 0$, the disk's surface density profile is initialized according to Equation 1.3. In the following time steps the planet is introduced to the disk.

To prevent disruptive shocks or numerical artifacts from arising at the introduction of the planet to the disk, its mass is first set to 0 and then slowly increased over the next few time steps. This time span will be referenced as *tapering period* hereafter. After the tapering period, the planet's mass then is equal to the inital mass value specified in the configuration files. The planet's intial velocity vector is set up in such a way as to position it on an orbit around the star.

To give the disk some time to settle into an equilibrium state, accretion does not start directly after the tapering has finished. Instead, the accretion subroutine is deactivated for a time span that shall be called *accretion wait*.

After the period of accretion wait is over, the planet can finally start gathering mass. This is realized in the code by an accretion subroutine, which consists of two parts. Both the *Kley* and *Machida* accretion rates, which will be explained in detail in just a minute, are calculated at each time step. Afterwards, the maximum value of these two is used to determine the amount of mass removed from the disk and added to the planet.

2.1.1 Accretion Mechanisms

To simulate gas accretion onto a planet, the following approach is used: After each time step Δt, a mass amount Δm is removed from the grid cells inside the Hill sphere and added to the planet.

$$m_{disk}(t + \Delta t) = m_{disk}(t) - \Delta m \tag{2.1}$$

$$m_{planet}(t + \Delta t) = m_{planet}(t) + \Delta m \tag{2.2}$$

The precise value of Δm is determined by making use of two different models, namely a slightly modified version of both the accretion recipe given by W. Kley et al. (1999) as well as the one given by M. Machida et al. (2010). Both accretion rates are calculated in each timestep, then the minimum of these two values is used.

$$\Delta m = \min\left(\Delta m_{Kley}; \ \Delta m_{Machida} \right) \tag{2.3}$$

Machida Accretion
Here, we use a variant of the Machida accretion formula utilized by himself in his 2006 paper [18]. In each time step, the amount of mass to be removed from the Hill sphere is given by

$$\Delta m_{Machida} = \Sigma(r, t) \cdot H^2 \cdot \Omega \cdot \min\left(0.14; \ 0.83 \cdot (r_H/H)^{9/2} \right) \cdot \Delta t \tag{2.4}$$

TODO: be more detailed?

Kley Accretion

Additionally to the Machida accretion, we will use a modified version of the accretion recipe suggested by W. Kley in his 1999 paper *Mass Flow and Accretion through gaps in Accretion Discs* [26]. The precise value of Δm is determined via

$$\Delta m = f_{red} \cdot S_{acc} \cdot \Sigma(r,t) \cdot f_{acc} \cdot \Delta t \tag{2.5}$$

Here, S_{acc} is the size of the disk surface inside the planet's Hill sphere, $\Sigma(r,t)$ is the gas surface density at a distance r from the planet's center at time t. With the parameter f_{acc}, the overall accretion rate can be tweaked and f_{red} determines from where precisely in the Hill sphere mass is removed. The latter is defined as

$$f_{red} = \begin{cases} \frac{2}{3} & \text{if } r/r_H < 0.45 \\ \frac{2}{3} \cdot \cos^4\left(r/r_H - 0.45\right) & \text{if } 0.45 \leq r/r_H \leq 0.95 \cdot \\ 0 & \text{if } r/r_H > 0.9 \end{cases} \tag{2.6}$$

A visualization of the r-dependence of f_{red} can be seen in Figure 2.2.
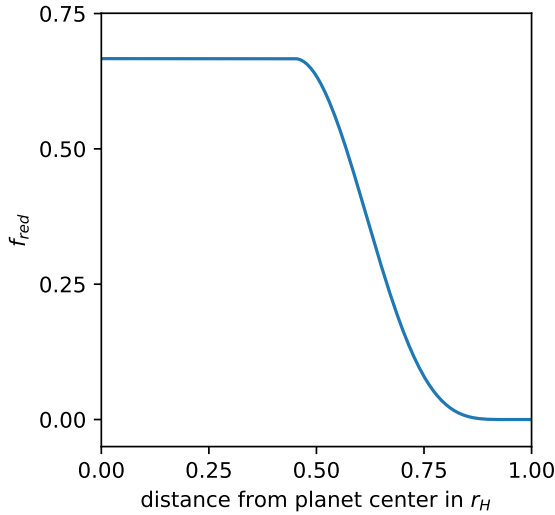
(a) r-dependence of f_{red}
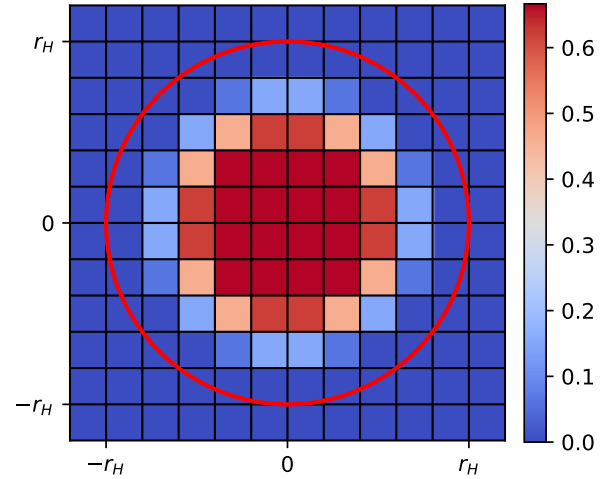
(b) Visualization of the value of f_{red} in the grid, the red circle marks the boundaries of the Hill sphere.

Figure 2.2: Smoothing function f_{red} that determines where and how much mass is to be taken by the Kley accretion subroutine out of the planetary Hill sphere at each time step.

2.1.2   Code Units

In astronomy, one often has to deal with large numbers, e.g. the solar mass is $M_\odot \approx 1.989 \times 10^{30}$ kg. In addition to making numbers less readable and harder to work with, using large numbers may also lead to bigger numerical errors [cite]. This can be avoided by choosing not to utilize SI units. Instead, a different system of measurement units is defined, which will be referenced as *code units* hereafter.

In this system, the basic measuring unit of mass is that of the sun, (i.e. $M_\odot = 1$). Spatial lengths are measured in multiples of the average distance between Jupiter and the sun, which in SI units amounts to about 5.2 au. All of the simulated planets in this thesis will be positioned at $r = 1$.

The mass of the central star is assumed to be much larger than that of the planet. Also, the Newtonian gravitational constant G is set to unity as well. Under these assumptions, the Keplerian angular velocity is simply $\Omega_K = 1$ and the period of one orbit of a planet (at $r = 1$) around the star is $T = 2\pi$.

The mass accretion rate $\dot{m}$ of a planet is measured in solar masses per orbit.

2.1.3   Default Parameters

If not otherwise specified, the following configuration values will be used by default:

Table 2.1: Default simulation parameters

parameter	value
aspect ratio h_r	0.05
flaring index β	0
surface density $\Sigma(r = 0)$	$3 \cdot 10^{-4}$
sigma slope γ	1
viscosity parameter α_{visc}	10^{-2}
mass tapering period	50 orbits
radial resolution N_{rad}	202
azimuthal resolution N_{sec}	456
lower boudary for 2D grid $R_{min,2D}$	0.2
upper boundary for 2D grid $R_{max,2D}$	5
lower boundary for 1D grid $R_{min,1D}$	0.02
upper boundary for 1D grid $R_{max,1D}$	50

2.2 First Runs

To get a general idea for the behavior of simulated disks over time, <mark>let us take a look at</mark> Figure 2.3. Here, a top-down view on the disk is shown, which is visualized in polar coordinates for various times. The color coding corresponds to the value of the the gas surface density on a logarithmic scale. The influence of the planet's momentum exchange with the gas is clearly visible in the forming spiral arms and the gap, which grows deeper and wider with time.

In Figure 2.4, an analogous plot can be seen, this time for a planet on an eccentric orbit ($e = 0.3$). Here, the disk evolvution is more chaotic. The gap formed by the planet is also much wider, which will be discussed in more detail later in this thesis, when the effect of the orbit eccentricity on the structure of the gap and therefore on the accretion rate will be investigated.

(a) after 50 orbits   (b) after 500 orbits   (c) after 2500 orbits
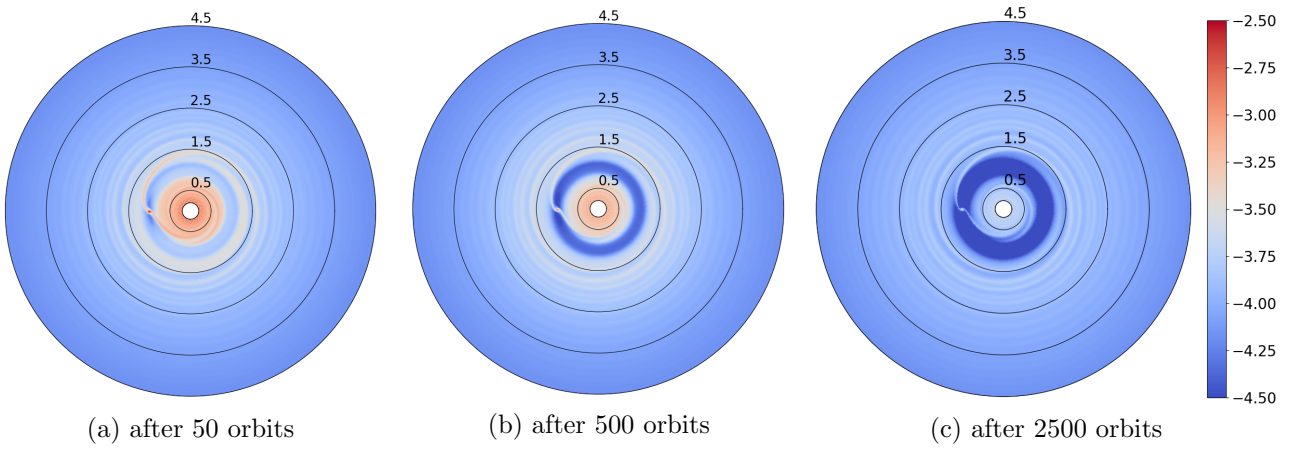
Figure 2.3: Evolution of gas surface density over time. A non-migrating, non-accreting planet of initial mass $m_0 = 1\ M_{jupiter}$ is put on a circular orbit. The disk parameters are $\alpha_{visc} = 10^{-2}$, $h_r = 0.05$. The exchange of angular momentum between gas and planet can be recognized by the formation of a gap in the disk.

(a) after 50 orbits   (b) after 500 orbits   (c) after 2500 orbits
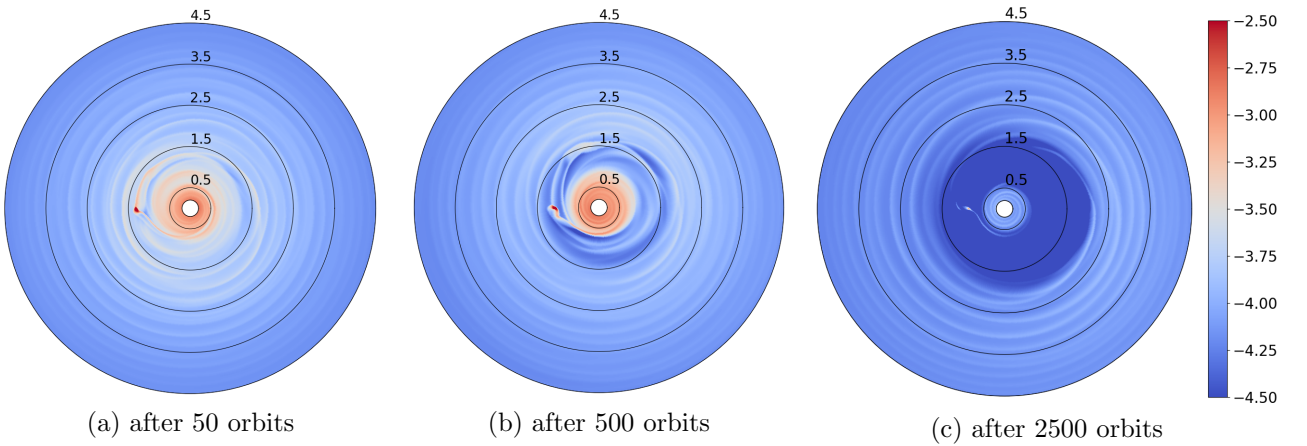
Figure 2.4: Evolution of gas surface density over time. A non-migrating, non-accreting planet of initial mass $m_0 = 1\ M_{jupiter}$ is put on an elliptic orbit of eccentricity $e = 0.3$. The disk parameters are $\alpha_{visc} = 10^{-2}$, $h_r = 0.05$. The exchange of angular momentum between gas and planet can be recognized by the formation of a gap in the disk, which is more wide than in the case of a circular orbit. The gap itself also possesses an eccentricity $e_{gap} \neq 0$, which increases both with e and m_0

2.3   Choosing the Resolution of the 2D1D-Grid

The *FARGO2D1D* algorithm defines resolution via the two variables N_{rad} and N_{sec}, which designate the number of grid cells in radial and azimuthal direction, respectively. To find the optimal simulation resolution, a compromise has to be found between the integration time and the accuracy of the simulation results. Before this is done though, the optimal ratio between the radial resolution N_{rad} and the azimuthal resolution N_{sec} has to be found:

The grid is treated by the algorithm simply as a 2D rectangular matrix. In reality though, the system is of course not rectangular, but circular. The projection of the rectangular grid into polar coordinates leads to a distortion of the square grid cells. The grid cells that are very close to the center as well as those very far away from the center are subject to strong distortions.

To make sure that the accretion subroutine functions accurately, the resolution should be chosen in such a way that the grid cells' shape is as close to a square as possible at the radial position of the planet (i.e. at $r = 1$). For that, let's take a look at Figure 2.5, which visualizes a radial grid section at a distance r from the center.
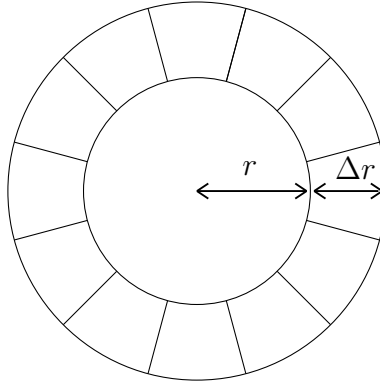
Figure 2.5: Sketch of a radial division in the simulation grid

To be as close to a square as possible, each azimuthal ring division should ideally have an area of

$$A_{cell} \approx \Delta r^2 \tag{2.7}$$

The total area of the ring is given by

$$A_{ring} = \pi(r + \Delta r)^2 - \pi r^2 = \pi(2r\Delta r + \Delta r^2) \tag{2.8}$$

Utilizing the relation $N_{sec} = A_{ring}/A_{cell}$ and then plugging in $r = 1$, this yields

$$N_{sec} = \pi\left(\frac{2}{\Delta r} + 1\right) \tag{2.9}$$

The width of the ring Δr can be determined from the radial resolution N_{rad} via

$$\Delta r = \frac{r_{max} - r_{min}}{N_{rad}} \tag{2.10}$$

Here, r_{min} and r_{max} denote the inner and outer radial boundaries of the 2D grid, which are set to $r_{min} = 0.2$ and $r_{max} = 5$ throughout this thesis. It should now be clear how to easily calculate the optimal value of N_{sec} for any value of N_{rad}. Still, a few test simulations need to be run before one can decide on the resolution which optimizes the trade-off between integration time and accuracy.

To get a sense of the resolution's influence on the accuracy of the results, simulations are to be run for multiple different resolutions, namely 2.5, 5 and 10 cells per Hill radius. For each number $N_{c/rH}$ of cells per Hill radius, N_{rad} can be calculated via

$$N_{rad} = N_{c/rH} \cdot \frac{r_{max} - r_{min}}{r_H} \tag{2.11}$$

From this, N_{sec} can be determined with Equation 2.9 and Equation 2.10. This yields:

Table 2.2: Radial and azimuthal resolutions for various numbers of grid cells per Hill radius

cells per r_H	N_{rad}	N_{sec}
2.5	101	230
5	202	456
10	404	909

Figure 2.6 visualizes how the planet's Hill sphere is implemented in the 2D array. For the simulations, a planet on a circular orbit with an intitial mass of 1 $M_{jupiter}$ is used, which builds up during a taper period of 10 orbits. After these 10 orbits, the planet starts accreting mass from its surroundings.

The radial gas density profile after a total of 500 orbits can be seen in Figure 2.7 on the next page. There is some discrepancy for small radii, but the overall structure of the gas density profile seems to be pretty much the same. To look at the behavior near zero, Figure 2.8 shows a zoomed in view of the disk. As can be seen here, a resolution of 2.5 cells per Hill radius leads to artifacts near the center, which disappear for higher resolution values.

Since the Hill radius increases with the planet's mass (see Equation 1.10), the number of grid cells inside the Hill radius will actually grow as time progresses and the planet accretes more material. Thus, these resolutions only form lower limits and get better over time. It has already been shown Lega et al. (2015) that at least 5 cells per Hill radius are necessary to accurately model planet migration. Because this resolution still offers the advantage of faster computation times by a factor 4 relative to having 10 cells per Hill radius, all subsequent simulations are run with

$$N_{rad} = 202 \text{ and } N_{sec} = 456$$

if not otherwise specified.
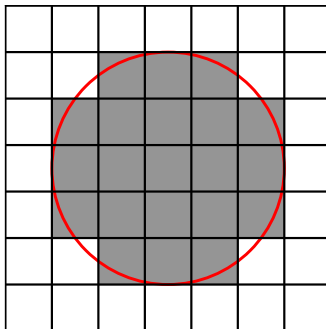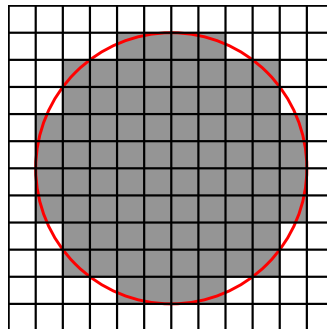
(a) 2.5 cells per r_H (b) 5 cells per r_H (c) 10 cells per r_H
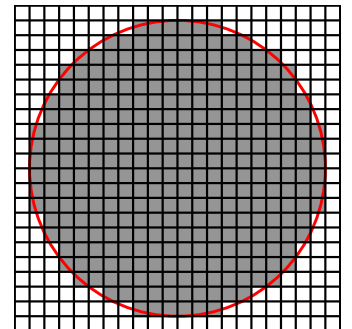
Figure 2.6: Visualization of Hill spheres in the grid for various resolutions
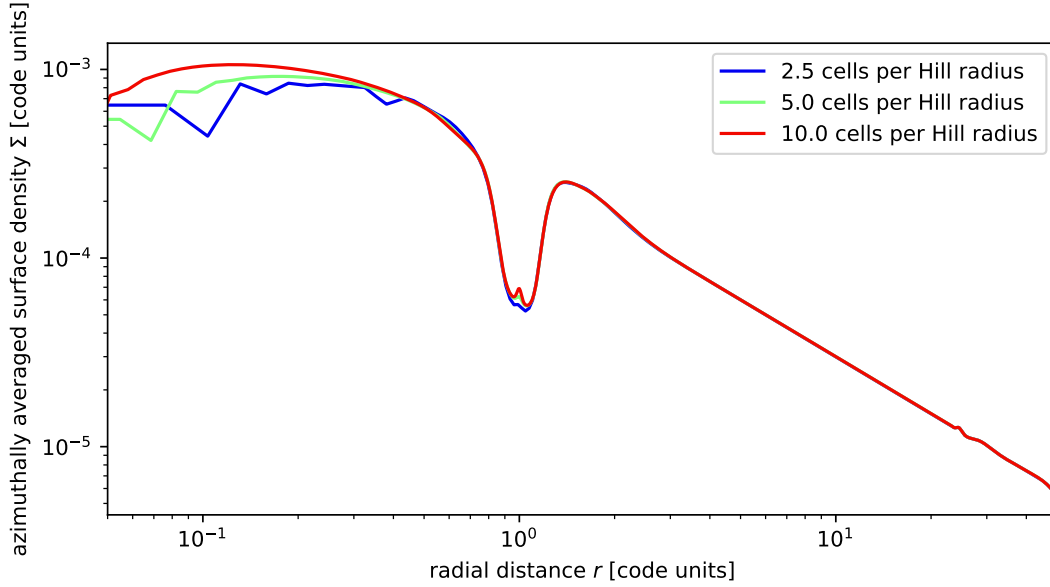
Figure 2.7: Azimuthally averaged surface densities at $t = 500$ orbits for three different grid resolutions. A single planet is positioned at $r = 1$. Its mass is initialized to $m_0 = 1\ M_{jupiter}$ during a tapering period of 5 orbits. Accretion starts at $t = 10$ orbits. Thus, the planet undergoes accretion for a total of 490 orbits. The planet is put on a circular orbit, migration is turned off and the disk is characterized by the parameters $\alpha_{visc} = 10^{-2}$, $h_r = 0.05$. The general structure of the gas density follows approximately the same course for all resolution values, with discrepancies being the largest for small values of r.
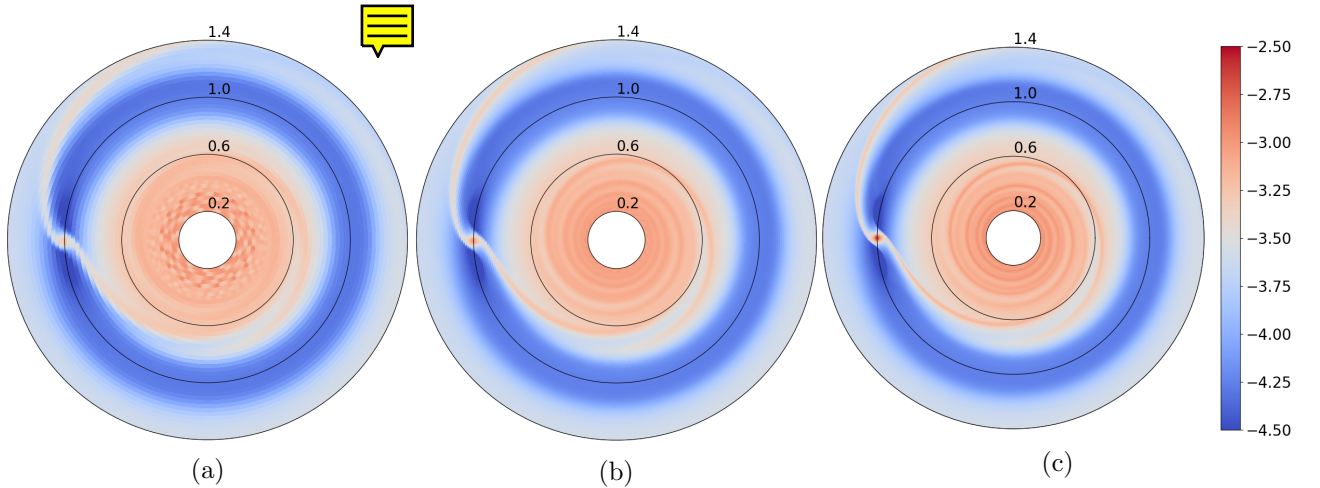
Figure 2.8: Gas surface density in the inner regions of the 2D grid for different resolutions at $t = 500$ orbits. The planet's mass is initialized to $m_0 = 1\ M_{jupiter}$ during a tapering period of 5 orbits. Accretion starts at $t = 10$ orbits. Thus, the planet undergoes accretion for a total of 490 orbits. The planet is put on a circular orbit and migration is turned off. The disk is characterized by the parameters $\alpha_{visc} = 10^{-2}$, $h_r = 0.05$. The black rings indicate the distance from the center, the color bar displays the order of magnitude (decadic logarithm) of the gas density in code units. For the lowest resolution, artifacts can be observed near the center of the disk, which disappear at higher resulution. Each doubling of the number of cells per Hill radius leads to a quadrupling of the needed computation time. Therefore, in this thesis we focus on simulations that initially have 5 grid cells per Hill radius.

2.4   Parameter Studies of the Disk

In this section, we investigate how the gas accretion rate onto the planet as well as the structure of the gap are influenced by the disk' characteristics, namely its geometry and the viscosity of the gas within the disk.

2.4.1   Disk Geometry

In our model, the geometry of the disk is mainly characterized by the aspect ratio h_r as well as the flaring index β. Let us first take a look at the influence of the aspect ratio. Simulations were carried out for various values of h_r with an integration time of 2500 orbits. During the first 50 orbits, the planet mass is slowly increased to 1 $m_{jupiter}$. Accretion starts at $t = 500$ orbits. The results can be seen in Figure 2.9a, where the gas density profile in the vicinity of the planet plotted as a function of the distance r from the disk center, and Figure 2.9, where the relative mass increase of the planet is plotted against h_r.

Higher values of the aspect ratio lead to a less deep gap, as has already been stated by Crida et al. (2006). This is to be expected, since in a thicker disk more material is available and therefore more gas diffuses into the forming gap, hindering the planet from depleting the region.

One would expect that the accretion rate of the planet increases with the amount of gas in its Hill sphere. This is exactly what we see in Figure 2.9b. Thicker disks lead to faster gas accretion onto a planet in the disk. Furthermore, it seems that the relationship between aspect ratio and accretion rate is a linear one, at least in this simplified model.

The influence of the flaring index β is of a similar kind. Since it determines the slope of the power law describing the gas surface density as a function r (see Equation 1.3), higher values of β correspond to more gas being available for accretion the vicinity of the planet.

Interestingly, the curves describing the surface density profile cross each other when varying the aspect ratio, but do not when varying the flaring index. Instead, Figure 2.10 shows what seems to be an additive offset between the gas profiles for different flaring indices. Increasing both h_r and β leads to a shallower gap, yet the surface density in disk regions around the gap grows with β and falls when increasing h_r.

Why is this?

Is it because β increases gas density throughout the whole disk, while h_r and α_{visc} (where the curves also cross) accelerate diffusion back into the gap?

(a) surface density vs. aspect ratio   (b) increase of mass vs. aspect ratio
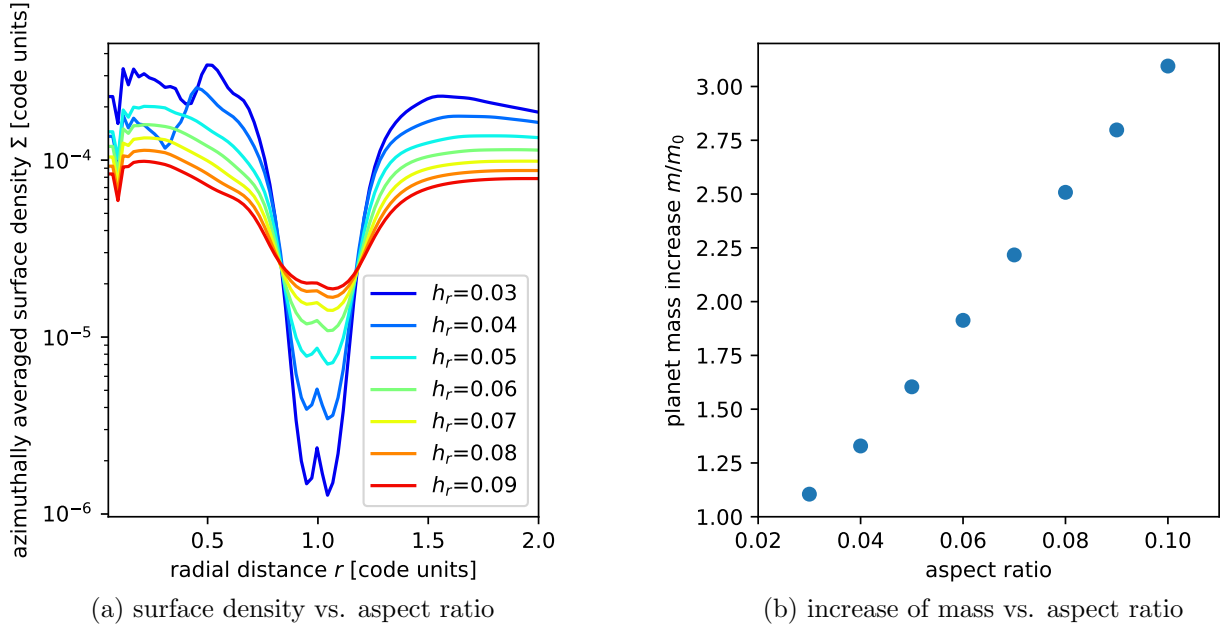
Figure 2.9: Influence of the disk's aspect ratio h_r on the gap profile and the increase of the planet's mass after an integration time of 2500 orbits. The first 50 of these orbits make up the tapering period (afterwards $m_0 = 1\ M_{jupiter}$) and the planet starts accreting after 500 orbits, the total duration of accretion is 2000 orbits. The planet is put on a circular orbit and migration is deactivated. The disk is characterized by the parameters $\alpha_{visc} = 10^{-2}$, $h_r = 0.05$. A thicker disk leads to more material diffusing into the forming gap, thus stifling its growth while accelerating accretion onto the planet.

(a) surface density vs. flaring index   (b) increase of mass vs. flaring index
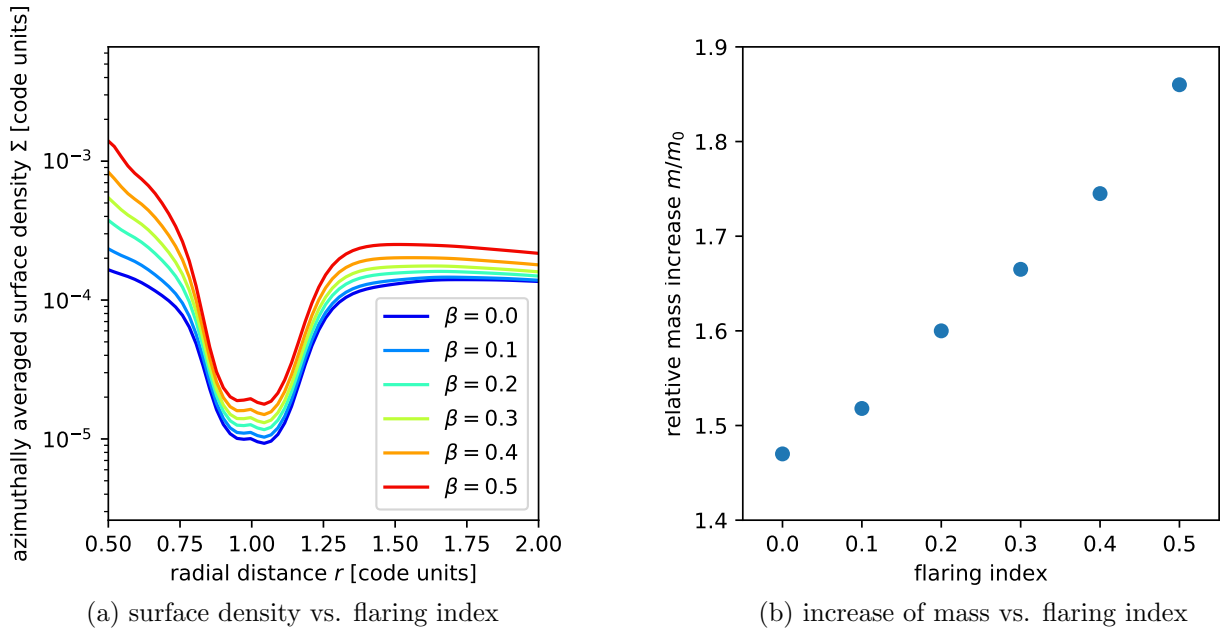
Figure 2.10: Gap profile and relative planet mass increase as a function of the disk's flaring index after an integration time of 2500 orbits. The first 50 of these orbits make up the tapering period (afterwards $m_0 = 1\ M_{jupiter}$) and the planet starts accreting after 500 orbits. Thus, the total accretion time has a duration of 2000 orbits. The planet is put on a circular orbit and migration is deactivated. The disk is characterized by the parameters $\alpha_{visc} = 10^{-2}$, $h_r = 0.05$. As overall more gas is available in the disk for higher values of β, the gap is less deep and the accretion rate increases.

2.4.2   Gas Viscosity Parameter

Next, we investigate the influence of the gas viscosity parameter α_{visc}. The simulations for this study were carried out using the same parameters as used in subsection 2.4.1, only this time the viscosity is not held constant. The aspect ratio is set to $h_r = 0.05$.

In Figure 2.11a, the gas surface density profile is plotted against the distance from the star. Large values of α_{visc} lead to a much less deep gap. While the planet's tidal influence due to gravity leads to a gas depletion in the regions close to its orbit, the material from further in- or outwards diffuses back in. If the gas is very viscous, this happens only slowly, and a gap can form. If, on the other hand, α_{visc} is large, the gap stays very shallow.

This is reflected in the relative mass increase that is plotted in Figure 2.11b. High values of α_{visc} lead to much more material being accreted by the planet, simply because there is that much more gas available in the its vicinity, analogous to what we saw for the parameter studies of the aspect ratio and flaring index.

TODO: explain why curves cross

(a) surface density vs. viscosity   (b) increase of mass vs. viscosity
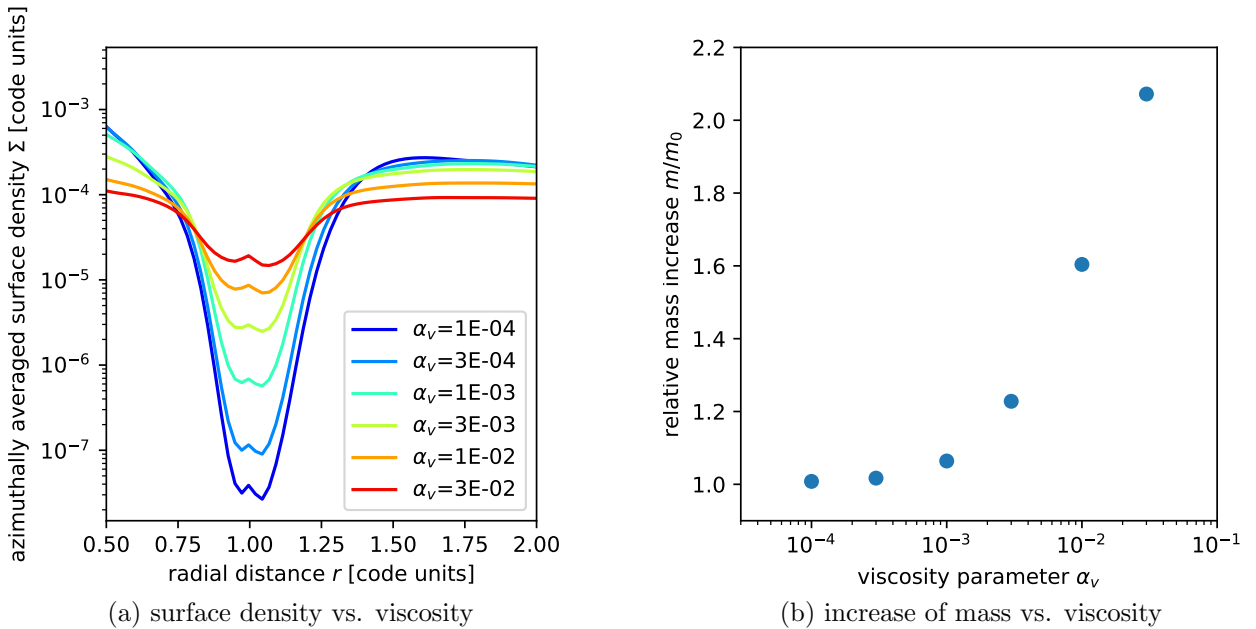
Figure 2.11: Influence of the disk's viscosity parameter α_{visc} on the gap profile as well the relative planet mass increase after an integration time of 2500 orbits. The first 50 of these orbits make up the tapering period (afterwards $m_0 = 1\ M_{jupiter}$) and the planet starts accreting after 500 orbits. Therefore, the planet undergoes accretion for a total of 2000 orbits. It is initialized on a circular orbit and migration is deactivated. The disk is characterized by the parameters $\alpha_{visc} = 10^{-2}$, $h_r = 0.05$. The depth of the gap decreases with the viscosity parameter. Less viscous disks supply a faster inflow of gas into the low density regions created by the planet. Accretion accordingly grows with α_{visc}.

2.5 Parameter Studies of the Planet

It would be great to gain insight into how the features of the planet effect its accretion rate. To do this, we first vary the initial mass of the planet after tapering. Afterwards, we take a look at the influence of the eccentricity of the planet's orbit.

In the code, the accretion rate itself can be tweaked by scaling it up or down by a multiplicative factor. This is investigated as well, to find out how the gap structure and planet mass increase behave for high rates of gas accretion.

2.5.1 Initial Planet Mass

In Figure 2.12, the structure of the gap is displayed for various different values of the initial planet mass. Just as one would expect from earlier investigations by e.g. Kley and Dirksen (2006), planets with a larger mass carve out a deeper gap due to their greater exchange of angular momentum with the gas.

The opening of the gap of course directly influences the amount of gas in the Hill region of the planet and therefore its gas accretion rate, as can be seen in Figure 2.13, where the absolute and relative mass increase is displayed against the initial mass. Figure 2.14 shows the mass increase against time.

Relative to their own intital mass, the smaller planets experience display the highest accretion rates.
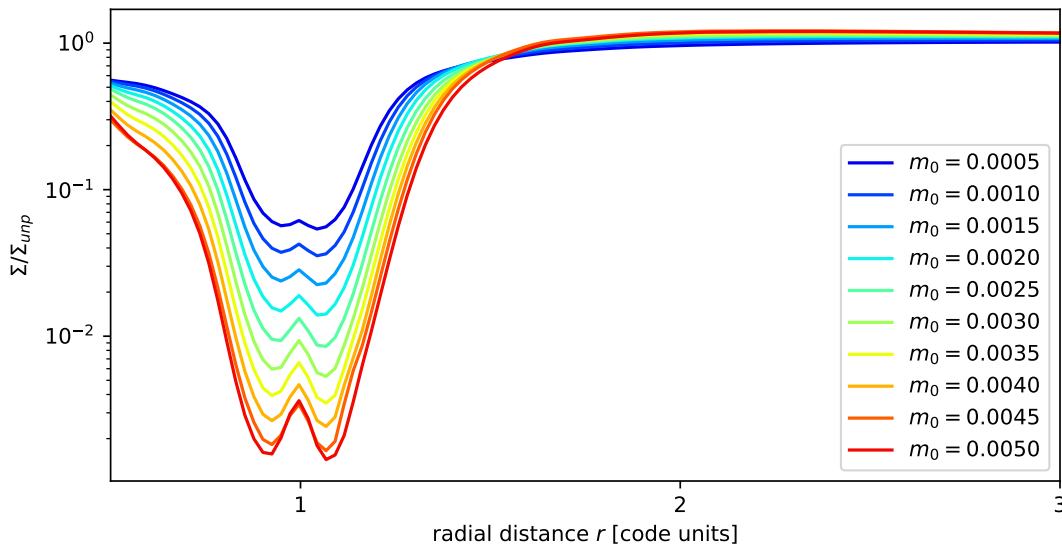
Figure 2.12: Surface density as a function of r for various initial planet masses after an integration time of 2500 orbits. The first 50 of these orbits make up the tapering period and the planet starts accreting after 500 orbits. Thus, the total accretion time has a duration of 2000 orbits. The planet is put on a circular orbit and migration is deactivated. The disk is characterized by the parameters $\alpha_{visc} = 10^{-2}$, $h_r = 0.05$. Due to their stronger interaction with the disk, high-mass planets carve out deeper and wider gaps than low-mass planets.

(a) absolute planet mass

(b) relative mass increase m/m_0
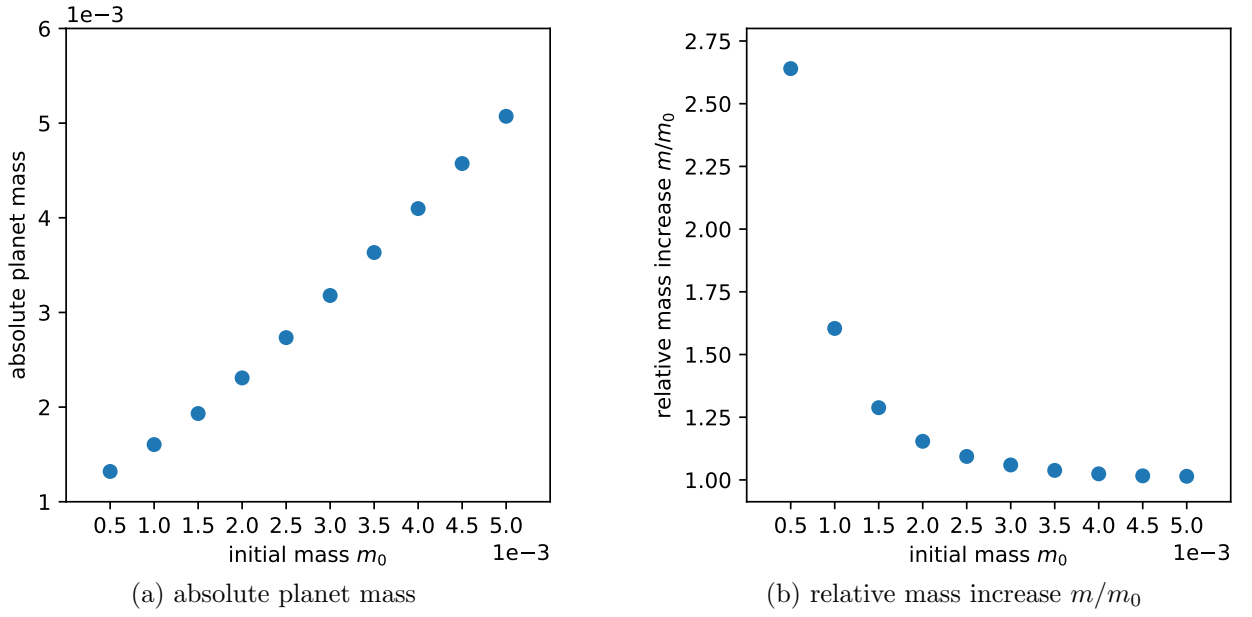
Figure 2.13: Absolute and relative mass increase of a planet for various initial masses. The total integration time is 2500 orbits, of which the first 50 orbits make up the tapering period and the planet starts accreting after 500 orbits. Thus, the total duration of accretion is 2000 orbits. The planet is put on a circular orbit and migration is deactivated. The disk is characterized by the parameters $\alpha_{visc} = 10^{-2}$, $h_r = 0.05$. Low-mass planets experience faster accretion due them creating only small gaps.

(a) mass increase vs. time and m_0

(b) accretion rate vs. time and m_0
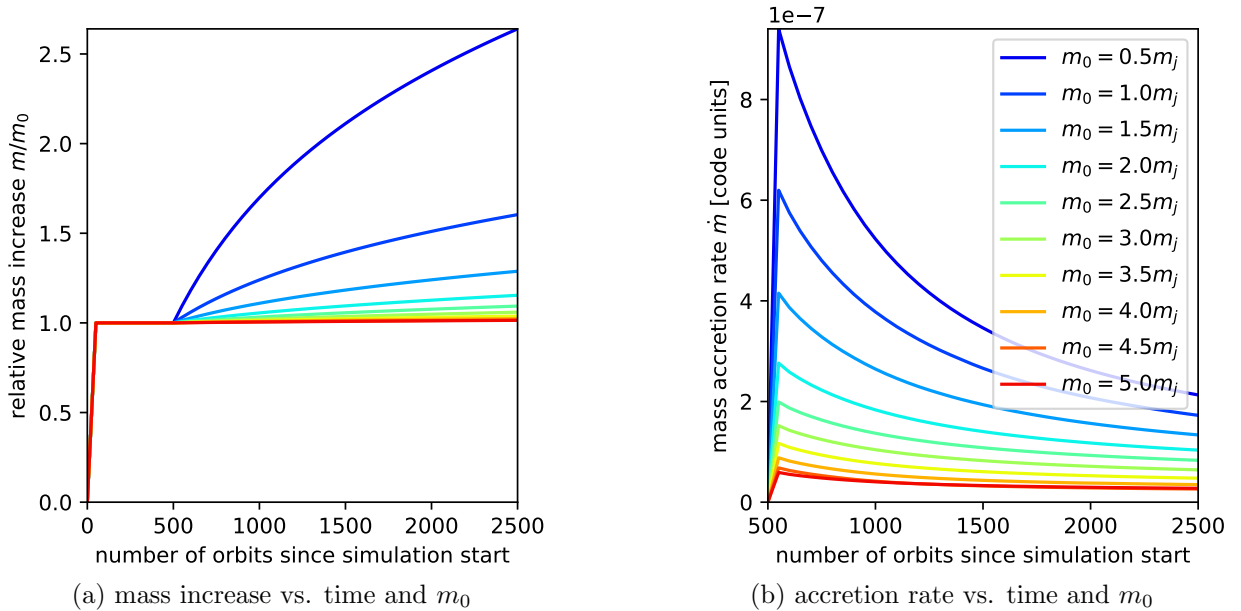
Figure 2.14: Relative mass increase and accretion rate as a function of time for different initial planet masses. The integration time is 2500 orbits, of which the first 50 orbits make up the tapering period, the planet starts accreting after 500 orbits. Thus, the planet experiences accretion for a total 2000 orbits. The planet is put on a circular orbit and migration is deactivated. The disk is characterized by the parameters $\alpha_{visc} = 10^{-2}$, $h_r = 0.05$. Planets accrete the fastest when they're still small, because the gap they create is much more shallow compared to more massive planets.

Gas Surface Density Profile At Time Of Equal Accretion

It would be interesting to see what the profile of the gap looks like at times of equal accretion for various planet masses. If the accretion rate is the same, then it would make sense if the amount of gas in the Hill sphere of the planet were similar or the same as well.

Let us look at points in time at which the accretion rate on a planet is equal to $3 \cdot 10^{-7}$ solar masses per orbit. Figure 2.15a attempts to visualize this. The times of interest are at the intersections between the black lines and the time axis. For each of these times, the surface density profile in the vicinity of the planet (divided by the unperturbed profile) is plotted in Figure 2.15b.

TODO: describe
plot mass in Hill sphere, similar?

(a) mass increase vs. time and m_0 (b) gap profile
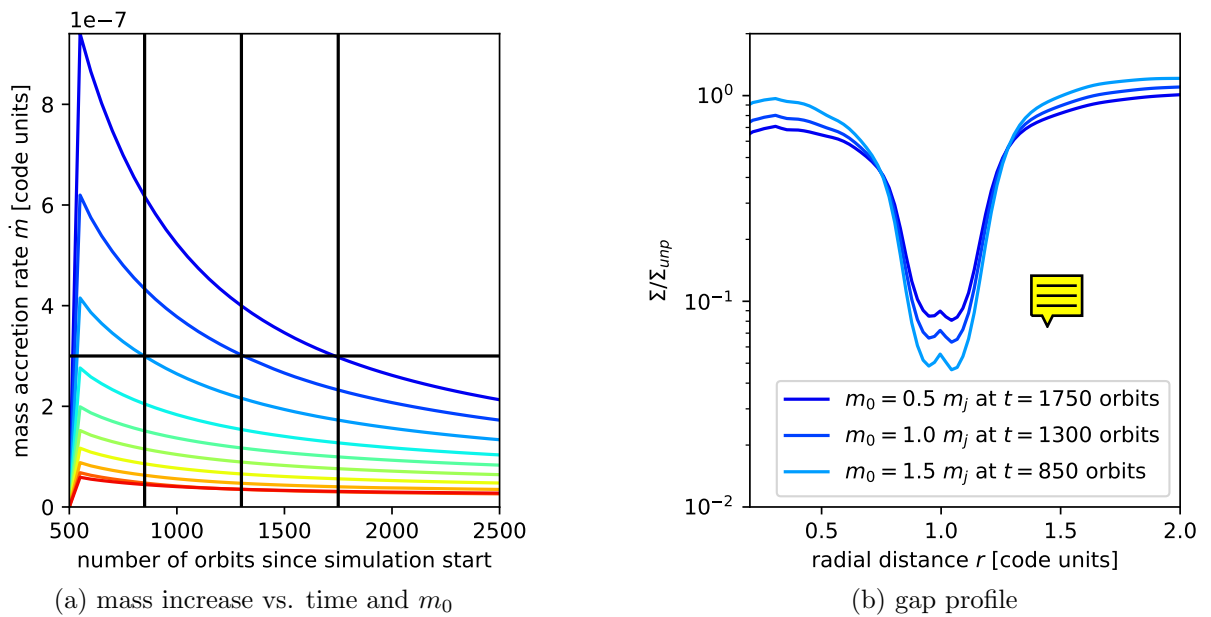
Figure 2.15: Comparison of gas density profiles at times of equal accretion. From the simulation results already shown in Figure 2.14a, we focus on the planets with the lowest mass, which meet the condition $\dot{m} = 3 \cdot 10^{-7}$ for different times. The gap profile is plotted for these times of equal accretion rates.

2.5.2   Numerical Accretion Rate

Let us take a look at the influence of the accretion rate of gas onto the planet, which can be tweaked in the code. Simulations are run for various factors between 0.5 and 3.0. The results can be seen in Figure 2.16.

As we increase the factor controlling the accretion rate, the gap grows deeper and the planet's mass increase grows larger, just as one would expect. It is interesting to see though that the relation between the relative mass increase and the accretion factor is not a linear one, but that the effect of the accretion factor on the mass increase seems to weaken for high values.

This is due to the eventual depletion of the Hill region. The relative mass increase is limited for very high accretion factors by the gas inflow into the gap from regions further in- or outwards.

(a) radial gas density vs. accretion   (b) mass increase vs. accretion
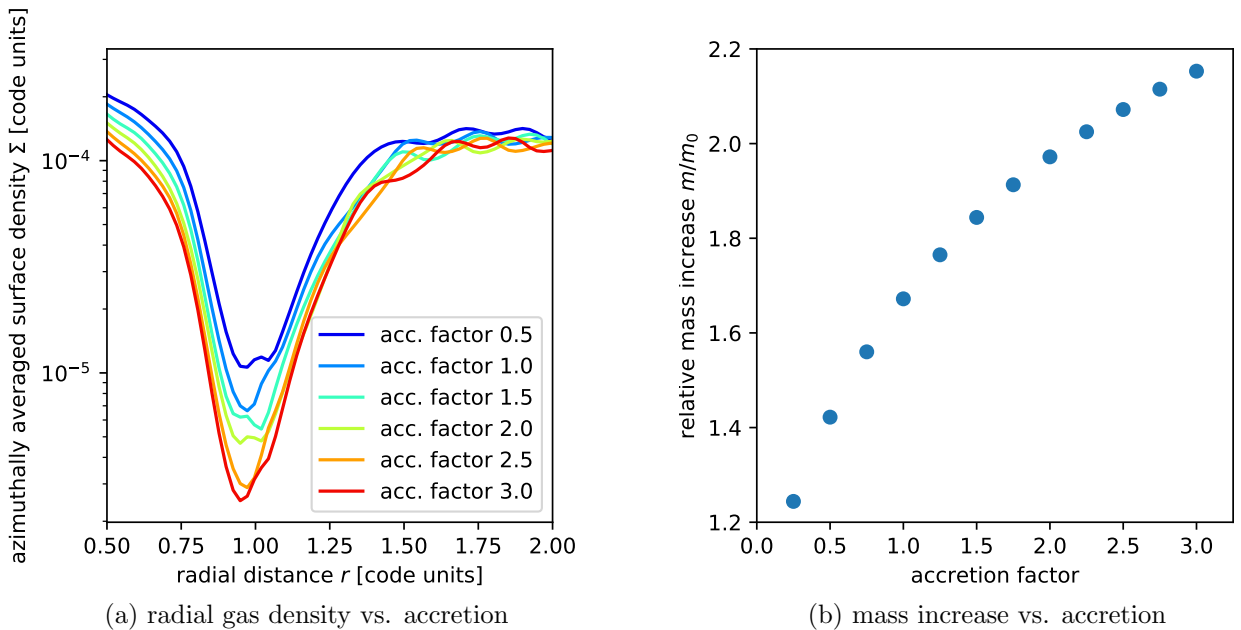
Figure 2.16: Influence of the numerical accretion rate on the gap profile and the planet's mass increase after the end of a simulation with an integration time of 2500 orbits. The first 50 of these orbits make up the tapering period and the planet starts accreting after 500 orbits. Thus, the total accretion time possesses a duration of 2000 orbits. The planet is put on a circular orbit and migration is deactivated. The disk is characterized by the parameters $\alpha_{visc} = 10^{-2}$, $h_r = 0.05$. High accretion rates lead to a large increase in planet mass, obviously. The effect is less noticable for high values of the accretion factor though, because the regions near the planet become more and more depleted and accretion slows down.

2.5.3   Initial Planet Eccentricity

Up until now, we've almost exclusively investigated planets on circular orbits. Let us now turn our attention towards planet orbit eccentricities $e \neq 0$. For the time being, the value of e is configured at the beginning of the simulation and then does not change over time, i.e. migration and eccentricity damping is turned off and the planet does not feel the gravitational potential of the disk, so that $e(t) = e_0 := e(t = 0)$. Simulations are run for various eccentricity values with an integration time of 2500 orbits. The first 50 orbits make up the tapering period and accretion is turned on at $t = 500$ orbits, after the gap has formed and the disk has reached a steady state.

Influence On The Profile Of The Gap
The surface density profile near the gap is plotted for $t = 500$ orbits (before accretion) in Figure 2.17a and for $t = 2500$ orbits (after accretion) in Figure 2.17b. Once again, the deepening of the gap over time via the planet's momentum exchange can be observed. Furthermore, it can be seen how the eccentricity influences the gap structure. Due to the periodic changes in the planet's distance from the star, the forming gap possesses a much wider profile for higher values of e_0. Consequently, its depth decreases for larger eccentricity values.

Figure 2.18 shows the azimuthally averaged surface density at the radial position of the planet (i.e. $\Sigma(r = 1)$) plotted against the eccentricity of the planet's orbit. TODO: Why is there a minimum?

(a) before accretion ($t = 500$ orbits)   (b) after accretion ($t = 2500$ orbits)
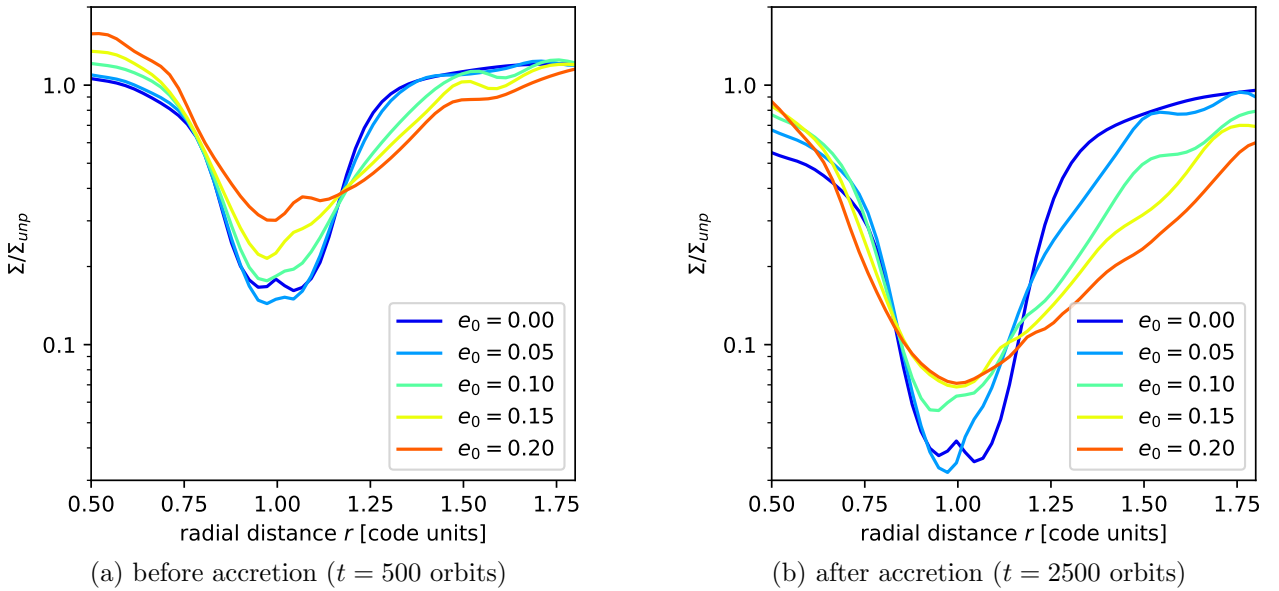
Figure 2.17: Surface gas density as a function of r for various planet orbit eccentricites. The left and right plot show the gap profile for two different times, namely before and after an accretion period of 2000 orbits. In the beginning, accretion is turned of. The first 50 orbits make up a tapering period (after which $m_0 = 1 \ M_{jupiter}$) and the planet starts accreting at $t = 500$ orbits. The total integration time therefore is 2500 orbits. Migration is deactivated and the disk is characterized by the parameters $\alpha_{visc} = 10^{-2}$, $h_r = 0.05$. The gap grows deeper with time, larger eccentricites lead to wider, yet more shallow gaps.

(a) before accretion $t = 500$ orbits

(b) after accretion ($t = 2500$ orbits)
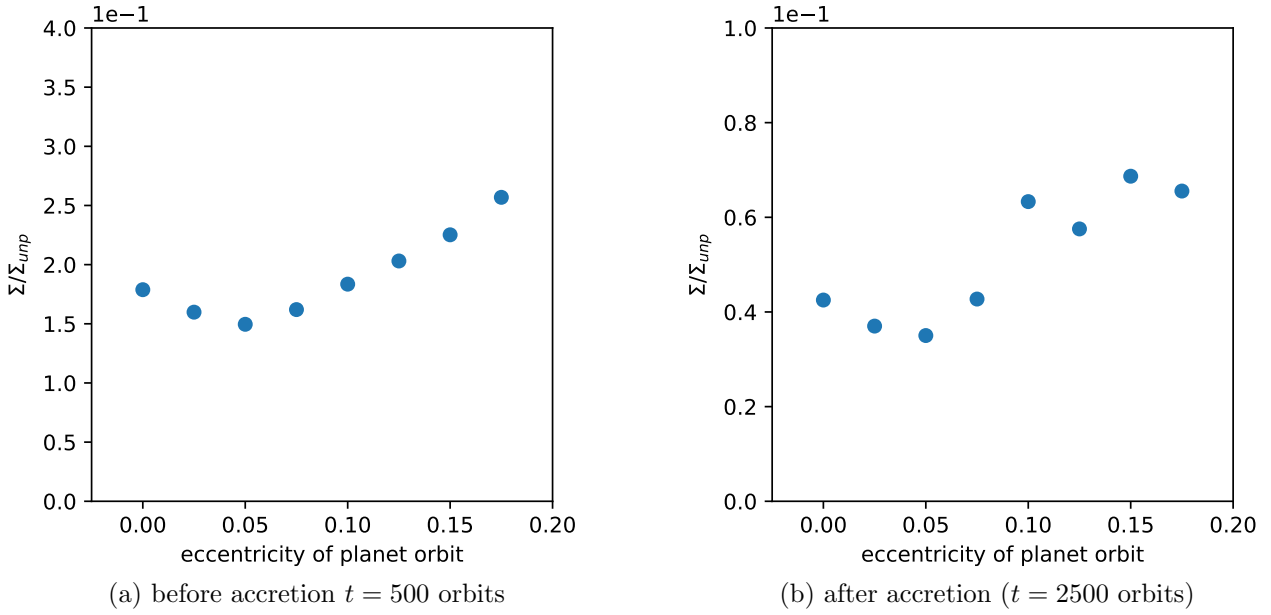
Figure 2.18: Gap depth (i.e. $\Sigma(r = 1)$) vs. planet orbit eccentricity. $t = 2500$ orbits. The first 50 orbits make up the tapering period, after which $m_0 = 1\ M_{jupiter}$. The planet starts accreting after 500 orbits, the planet therefore undergoes accretion for a total of 2000 orbits. Migration is deactivated and the disk is characterized by the parameters $\alpha_{visc} = 10^{-2}$, $h_r = 0.05$. This helps visualize why planets on eccentric orbits accrete at a higher rate than those on cirular orbits, since there is more material in the immediate vicinity of the planet.
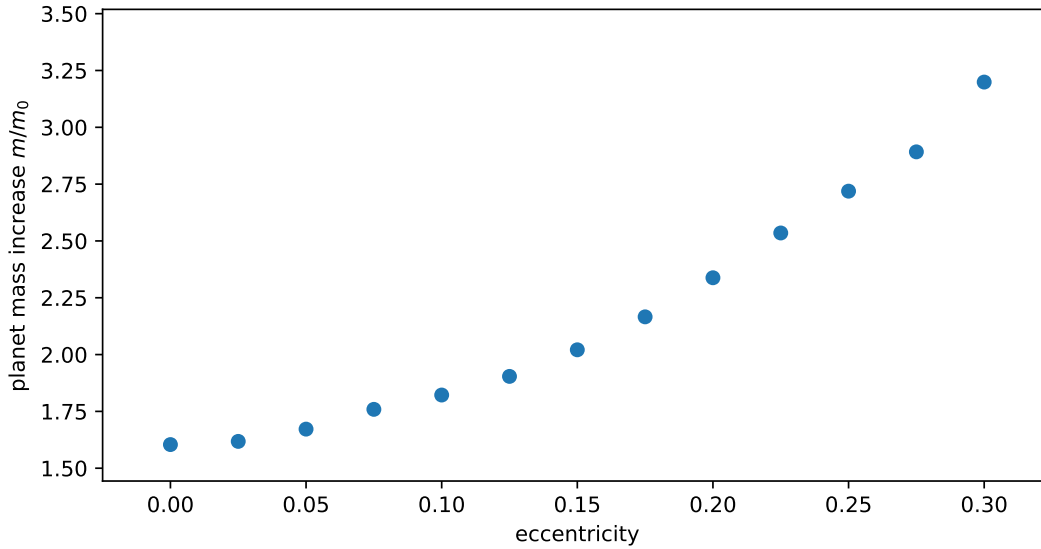
Figure 2.19: Relative planet mass increase as a function of orbit eccentricity at $t = 2500$ orbits. The first 50 of these orbits make up the tapering period, after which $m_0 = 1\ M_{jupiter}$. The planet starts accreting after 500 orbits. Thus, the total accretion time possesses a duration of 2000 orbits. Migration is deactivated and the the disk is characterized by the parameters $\alpha_{visc} = 10^{-2}$, $h_r = 0.05$. Planets on high-eccentricity orbits accrete faster than those on low-eccentricity or cirular orbits.

Influence On Accretion

The relative mass increase m/m_0 after 2000 orbits of accretion is plotted against the orbit eccentricity of the planet in Figure 2.19. Here, the effect of the shallower gap can be seen clearly, as planets on orbits of high eccentricity accrete drastically more gas than those on near-circular or circular orbits.

The evolution of the planet's mass over time is plotted in Figure 2.20a, where we can see how the intially fast mass increase slows down over time as the gap forms. The accretion rate, plotted in Figure 2.20b against time, seems to be converging towards a common limiting value.

To further look into this, a set of simulations is run with an integration time of 50000 orbits. The resulting temporal evolutions of m/m_0 and $\dot{m}$ are displayed in Figure 2.21 on the next page. The limiting value of the accretion rate is determined by the speed at which gas flows back into the gap from the surrounding regions. It is therefore strongly dependent on the gas viscosity.

TODO: determine limiting value
Why is $e = .05$ behaving differently? $e = 0.1$ also falls of at the end

(a) mass increase vs. time and e_0 (b) accretion rate vs. time and e_0
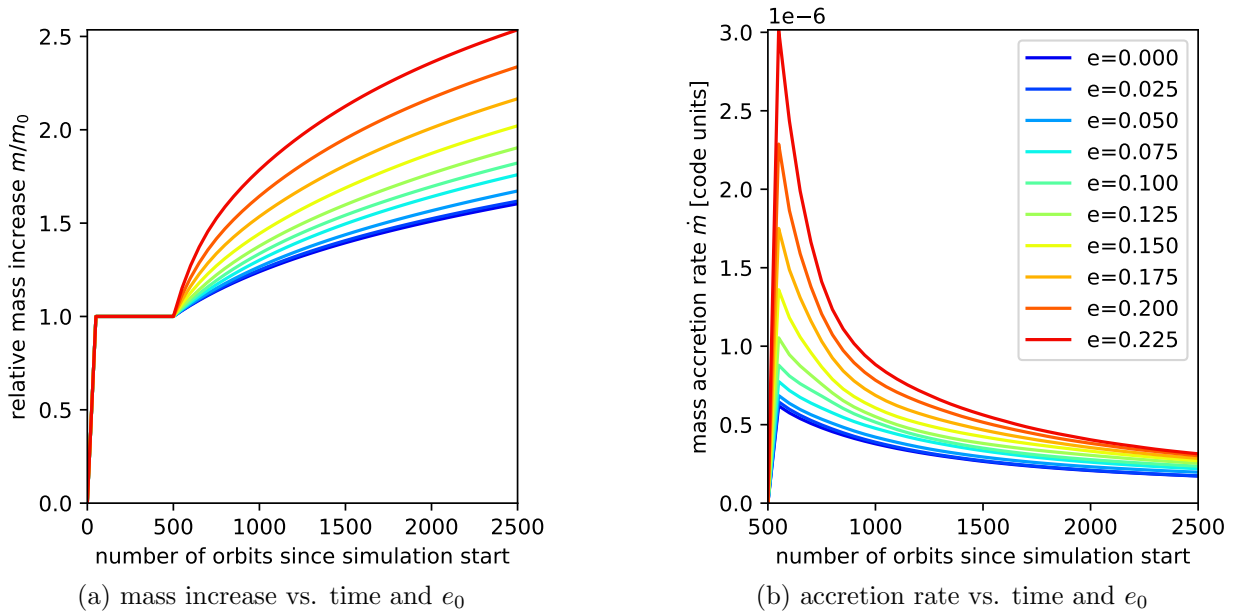
Figure 2.20: Influence of the planet eccentricity on the relative mass increase as well as accretion rate during a simulation with an integration time of 2500 orbits. The first 50 of these orbits make up the tapering period, after which $m_0 = 1\ M_{jupiter}$. The planet starts accreting after 500 orbits. Thus, the total duration of accretion is 2000 orbits. Migration is deactivated and the disk is characterized by the parameters $\alpha_{visc} = 10^{-2}$, $h_r = 0.05$. Planets on high-eccentricity accrete gas faster, yet for all values of e_0 the rate of accretion decreases with time as the gap is depleted of the gas. The accretion rate approaches a minimum value determined by the inflow of gas from distant regions into the gap, which depends heavily on the gas viscosity.

(a) mass increase vs. time and e_0 (b) accretion rate vs. time and e_0
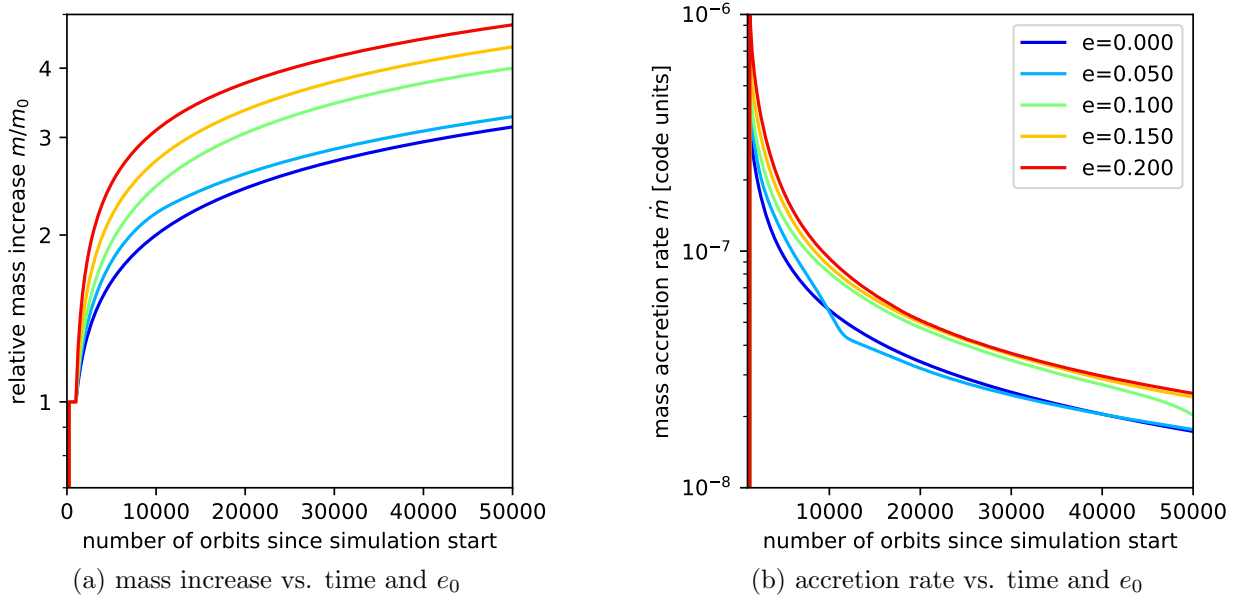
Figure 2.21: Long term evolution: Relative mass increase and accretion rate as a function of time for different orbit eccentricities (plotted logarithmically). The mass of the planet is initialized to $m_0 = 1\ M_{jupiter}$ during a tapering period of 50 orbits, it starts accreting after 1000 orbits. Thus, the total accretion time is 49000 orbits. Migration is deactivated and the disk is characterized by the parameters $\alpha_{visc} = 10^{-2}$, $h_r = 0.05$. The accretion rate falls off over time and approaches a limiting value determined by the speed at which gas from the surrounding regions can flow back into the gap.

(a) gap eccentricity vs. initial planet eccentricity   (b) gap eccentricity vs. initial planet mass
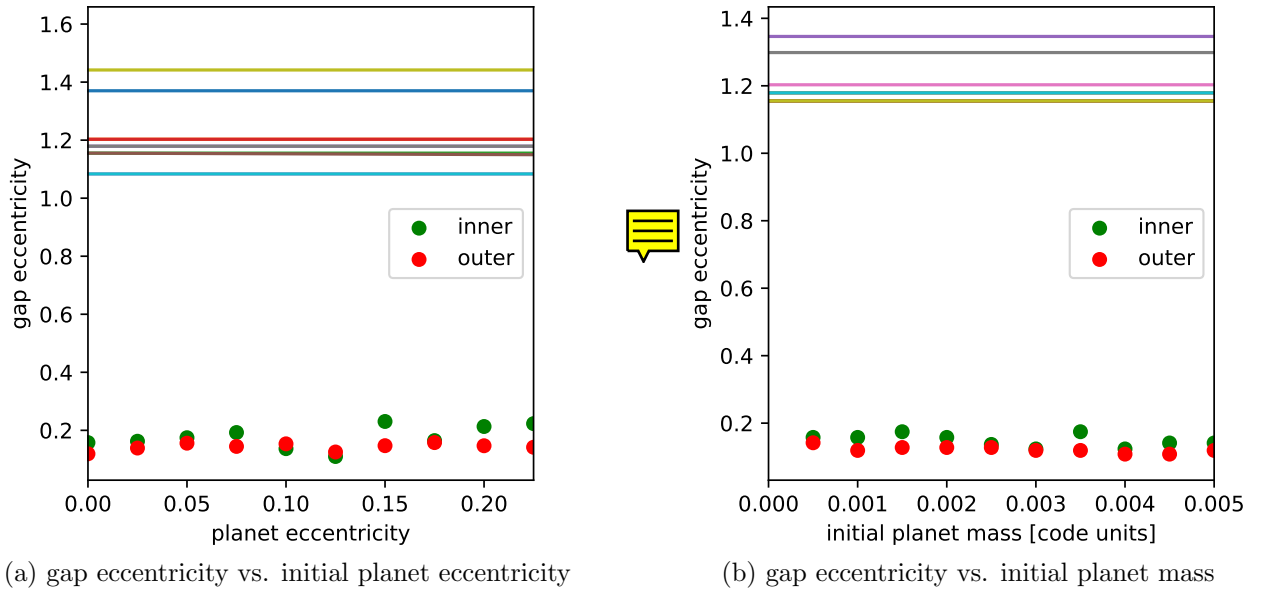
Figure 2.22: Gap eccentricity as a function of the planet's orbit eccentricity and planet mass (plotted at $t = 2500$ orbits). The first 50 of these orbits make up the tapering period and the planet starts accreting after 100 orbits. Thus, the total accretion time has a duration of 2000 orbits. When varying eccentricity, the initial mass of the planet is set to $m_0 = 1\ M_{jupiter}$. When varying the mass, the initial orbit eccentricity is $e_0 = 0$. Migration is deactivated. The disk is characterized by the parameters $\alpha_{visc} = 10^{-2}$, $h_r = 0.05$. (ignore content of plot for now)

Gap Eccentricity

- gap boundaries can be calculated from minima and maxima of the gas pressure in the disk

- Crida 2006

- eccentricity can be calculated from semimajor and semiminor axes a and b

$$e = \frac{a + b}{a - b} \tag{2.12}$$

- alternatively, gap eccentricity can also be calculated by defining defining the gap as all grid cells with $\Sigma/\Sigma_0 < 0.2$, treating them all as seperate free particles with individial orbit eccentricities, and taking the mean of all the eccentricities, already done by Hosseinbor et al. (2007)

(Something seems to be wrong with the way I determine gap boundaries from pressure gradients, still need to be fix this over the next few days. This should be the last big hurdle...)

2.6 Investigating a Migrating Planet

So far, the orbit eccentricity as well as the semimajor (and semiminor) axis have been assumed to be invariant in time to better study the influences of the various disk and planet parameters. For this, the planet was modeled in such a way as not to feel the gravitational influence of the gas particles in the disk.

When attempting to accurately model the evolution of a proto-planetary disk, this interaction should not be neglected, since it can lead to changes in the planet's semimajor axis and eccentricity, which then again influence the planet formation processes.

A non-accreting planet of varying mass and eccentricity is placed in orbit around the star. In the beginning the planet feels only the potential of the star, therefore no migration occurs. The disk does feel the planet though, so that a gap forms. We wait until a steady gap is reached after 500 orbits and then make two sets of simulations, once with accretion turned on and once with it turned off.

Figure 2.24 and Figure 2.23 show the temporal evolution of the semimajor axis for various masses and eccentricities. TODO: explain

...

The eccentricity damping over time can be seen in Figure 2.25 and Figure 2.26 on the next page for various masses and eccentricities. The overall evolution for accreting and non-accreting is relatively similar, as has already been observed by Stoll and Kley (2014)

TODO: explain

(a) without accretion   (b) with accretion
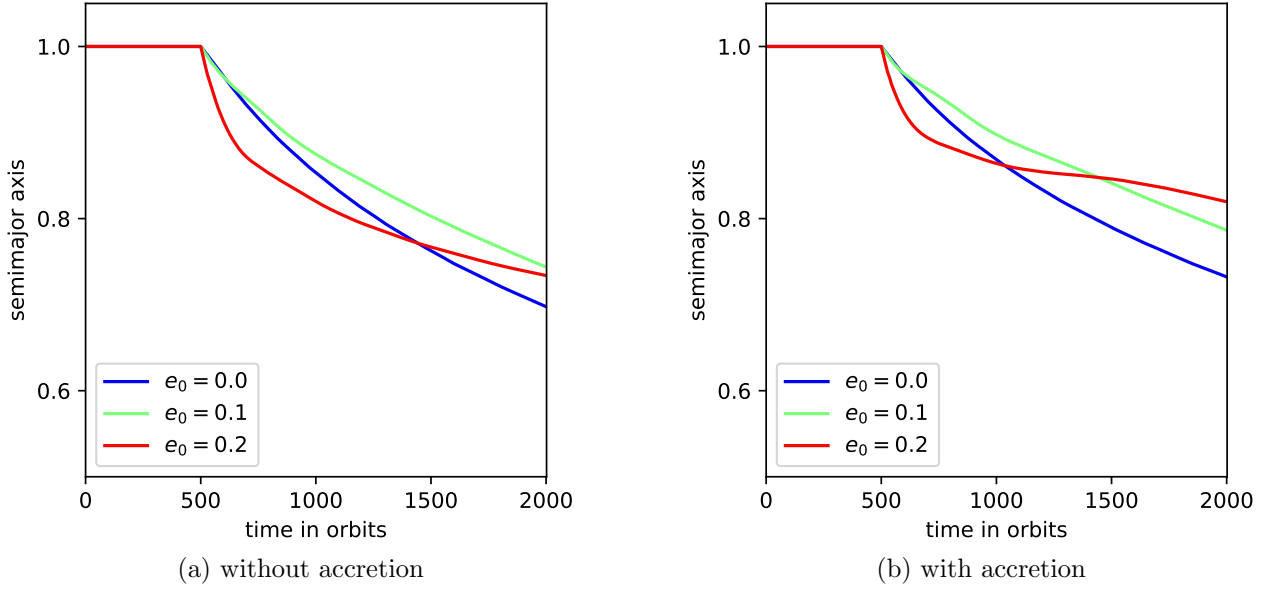
Figure 2.23: Temporal evolution of a migrating planet's semimajor axis for various values of the initial orbit eccentricity during an integration time of 2500 orbits. The first 50 of these orbits make up the tapering period (after which $m_0 = 1\ M_{jupiter}$) and the planet starts accreting after 100 orbits. Thus, the total accretion time possesses a duration of 2000 orbits. The disk is characterized by the parameters $\alpha_{visc} = 10^{-2}$, $h_r = 0.05$. (TODO: describe)

(a) without accretion   (b) with accretion
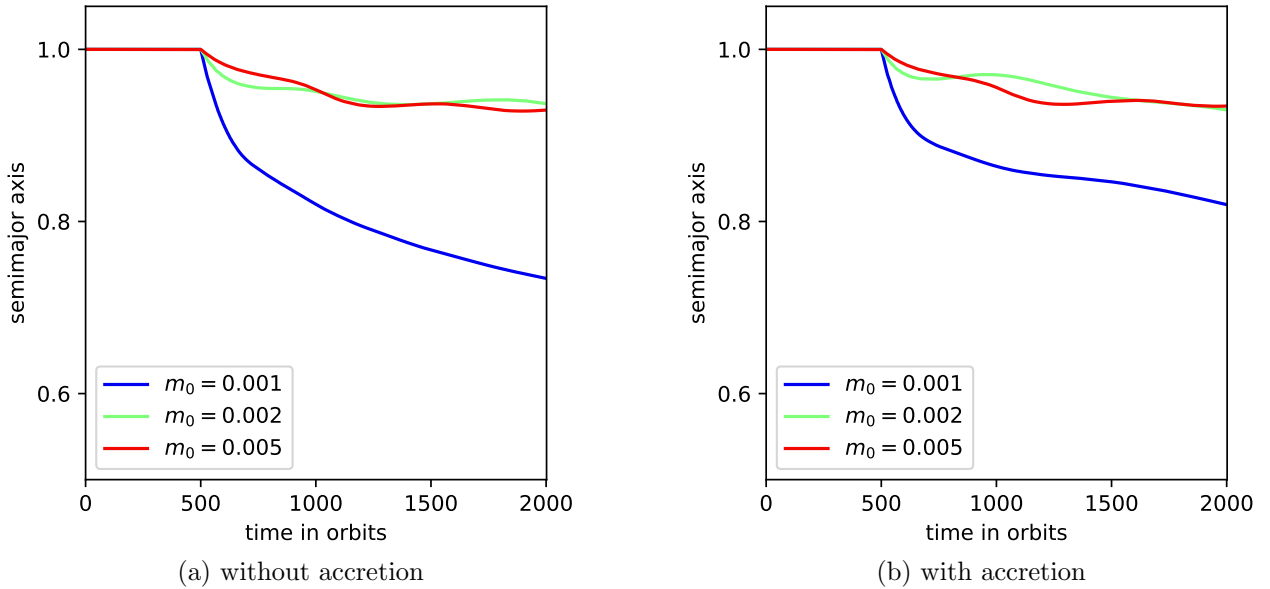
Figure 2.24: Temporal evolution of a migrating planet's semimajor axis for different values of the initial planet mass during an integration time of 2500 orbits. The first 50 of these orbits make up the tapering period (after which $m_0 = 1\ M_{jupiter}$) and the planet starts accreting after 100 orbits. Thus, the total accretion time possesses a duration of 2000 orbits. The disk is characterized by the parameters $\alpha_{visc} = 10^{-2}$, $h_r = 0.05$. (TODO: describe)

(a) without accretion

(b) with accretion
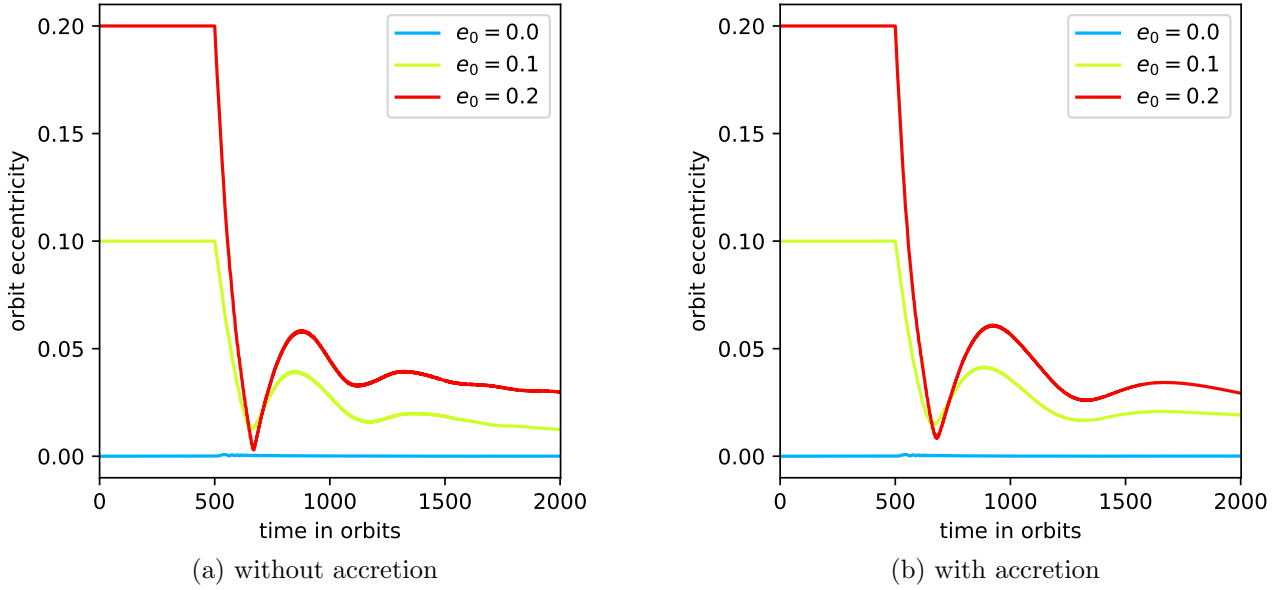
Figure 2.25: Temporal evolution of the orbit eccentricity of a migrating planet for different orbit eccentricites during an integration time of 2500 orbits. The mass of the planet is initialized to $m_0 = 1\ M_{jupiter}$ during a tapering period of 50 orbits. Accretion starts at $t = 100$ orbits. Thus, the planet accretes for a total of 2000 orbits. The disk is characterized by the parameters $\alpha_{visc} = 10^{-2}$, $h_r = 0.05$. (TODO: describe)

(a) without accretion

(b) with accretion
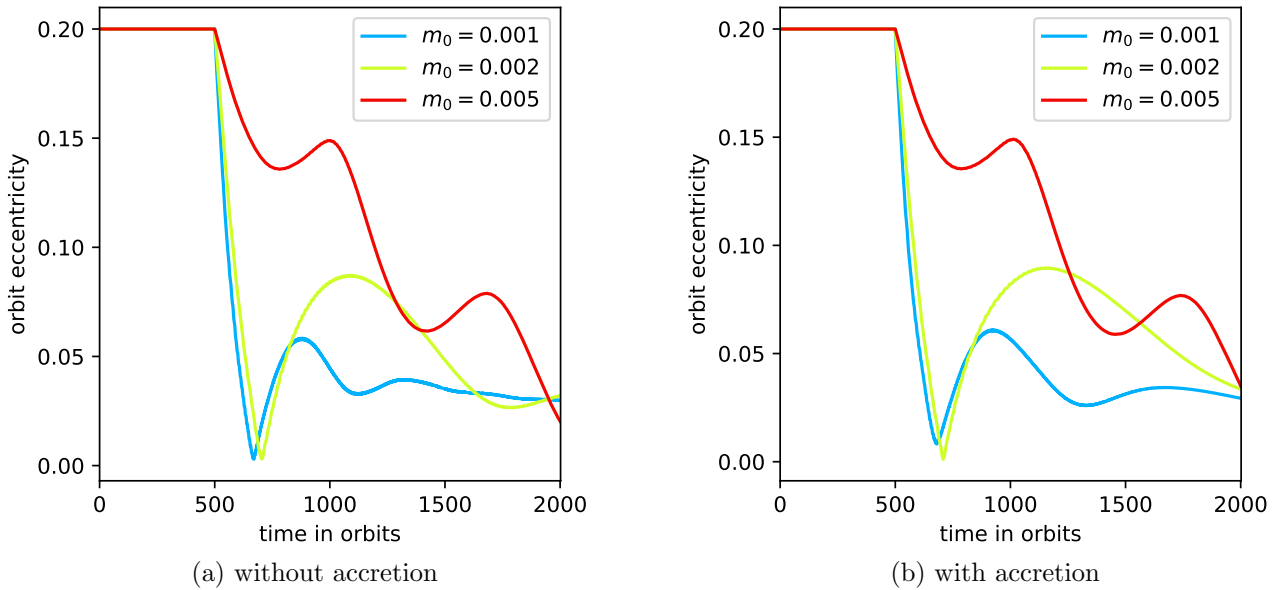
Figure 2.26: Temporal evolution of the orbit eccentricity of a migrating planet for various different initial masses during an integration time of 2500 orbits. The mass of the planet is initialized to $m_0 = 1\ M_{jupiter}$ during a tapering period of 50 orbits. Accretion starts at $t = 100$ orbits. Thus, the planet accretes for a total of 2000 orbits. The disk is characterized by the parameters $\alpha_{visc} = 10^{-2}$, $h_r = 0.05$. (TODO: describe)

Chapter 3

# Results

In this thesis, several studies were done regarding the accretion of gas in proto-planetary disks onto planets on eccentric orbits. The *FARGO2D1D* algorithm was used to simulate a thin, locally isothermal alpha disk.

It could be shown a planet's orbit eccentricity greatly influences the gas surface density profile of the gap formed due to exchange processes of angular momentum between disk and planet. Orbits of high eccentricities lead to the formation of much more shallow gaps, whose radial extension is accordingly greater.

This in turn directly influences the amount of gas present in the vicinity of the planet's orbit. To be more precise, the total amount of gas inside the Hill sphere of a planet on an eccentric orbit is larger than it would be for a planet on a circular orbit.

Thus, eccentric planets undergo gas accretion at a faster rate.

TODO: talk about migration, eccentricity damping

- various disk parameter's influence on gap formation, including

    - gas viscosity
    - disk geometry (aspect ratio and flaring index)
    - planet mass
    - planet orbit eccentricity

Chapter 4

Discussion

- compare to planet population synthesis (Bitsch 2018)
  von wem war nochmal das andere Paper? das hier?
  `http://www.mpia.de/homes/ppvi/chapter/benz.pdf`

-

- only relevant for planets massive enough to form a gap, yet still in a gap with enough free material to allow accretion

-

- lots of stuff neglected (MHD, radiation, temperature differences...)

-

Chapter 5

Appendix

5.1 References

[1] ALMA (ESO/NAOJ/NRAO). *ALMA image of the protoplanetary disc around HL Tauri*. URL: https://www.eso.org/public/archives/images/original/eso1436a.tif. (accessed: 11.02.2020).

[2] S. Andrews (Harvard-Smithsonian CfA); B. Saxton (NRAO/AUI/NSF); ALMA (ESO/NAOJ/NRAO). *ALMA image of the disc around the young star TW Hydrae*. URL: https://www.eso.org/public/archives/images/original/eso1611a.tif. (accessed: 11.02.2019).

[3] K. Baillié, S. Charnoz, and E. Pantin. "Trapping planets in an evolving protoplanetary disk: preferred time, locations, and planet mass". In: *Astronomy & Astrophysics* 590 (May 2016), A60. ISSN: 1432-0746. DOI: 10.1051/0004-6361/201528027. URL: http://dx.doi.org/10.1051/0004-6361/201528027.

[4] T. Birnstiel, C. P. Dullemond, and F. Brauer. "Gas- and dust evolution in protoplanetary disks". In: *Astronomy and Astrophysics* 513 (Apr. 2010), A79. ISSN: 1432-0746. DOI: 10.1051/0004-6361/200913731. URL: http://dx.doi.org/10.1051/0004-6361/200913731.

[5] D.P. Hamilton & J.A. Burns. "Orbital stability zones about asteroids. II - The destabilizing effects of eccentric orbits and of solar radiation". In: *Icarus* 96.1 (1992), pp. 43–64. DOI: https://www.sciencedirect.com/science/article/pii/001910359290005R.

[6] C.P. Dullemond and J.D. Monnier. "The Inner Regions of Protoplanetary Disks". In: *Annual Review of Astronomy and Astrophysics* 48.1 (Aug. 2010), pp. 205–239. ISSN: 1545-4282. DOI: 10.1146/annurev-astro-081309-130932. URL: http://dx.doi.org/10.1146/annurev-astro-081309-130932.

[7] C. Dürmann and W. Kley. "Migration of massive planets in accreting disks". In: *Astronomy & Astrophysics* 574 (Jan. 2015), A52. ISSN: 1432-0746. DOI: 10.1051/0004-6361/201424837. URL: http://dx.doi.org/10.1051/0004-6361/201424837.

[8] F. Masset. "FARGO: A fast Eulerian Transport Algorithm for Differentially Rotating Disks". In: *Astron. Astrophys. Supp. Series* (1999). DOI: 10.1051/aas:2000116.

[9] FARGO3D. *2D1D grid*. [Online; accessed January 06, 2020]. URL: http://fargo.in2p3.fr/local/cache-vignettes/L500xH501/gif_1D2Dgrid-352ab.png.

[10] FARGO3D. *What is FARGO2D1D?* URL: http://fargo.in2p3.fr/What-is-FARGO-2D1D. (accessed: 17.01.2020).

[11]   A. Pasha Hosseinbor et al. "The formation of an eccentric gap in a gas disc by a planet in
        an eccentric orbit". In: *Monthly Notices of the Royal Astronomical Society* 378.3 (June 2007),
        pp. 966–972. ISSN: 1365-2966. DOI: 10.1111/j.1365-2966.2007.11832.x. URL: http:
        //dx.doi.org/10.1111/j.1365-2966.2007.11832.x.

[12]   M. Keppler et al. "Discovery of a planetary-mass companion within the gap of the transition
        disk around PDS 70". In: *Astronomy & Astrophysics* 617 (Sept. 2018), A44. ISSN: 1432-0746.
        DOI: 10.1051/0004-6361/201832957. URL: http://dx.doi.org/10.1051/0004-6361/
        201832957.

[13]   A. R. King, J. E. Pringle, and M. Livio. "Accretion disc viscosity: how big is alpha?" In: *Monthly
        Notices of the Royal Astronomical Society* 376.4 (Mar. 2007), pp. 1740–1746. ISSN: 1365-2966.
        DOI: 10.1111/j.1365-2966.2007.11556.x. URL: http://dx.doi.org/10.1111/j.1365-
        2966.2007.11556.x.

[14]   W. Kley and G. Dirksen. "Disk eccentricity and embedded planets". In: *Astronomy & Astro-
        physics* 447.1 (Jan. 2006), pp. 369–377. ISSN: 1432-0746. DOI: 10.1051/0004-6361:20053914.
        URL: http://dx.doi.org/10.1051/0004-6361:20053914.

[15]   D. N. C. Lin and J. C. B. Papaloizou. "On the Tidal Interaction Between Protostellar Disks
        and Companions". In: *Protostars and Planets III*. Ed. by Eugene H. Levy and Jonathan I.
        Lunine. Jan. 1993, p. 749.

[16]   D. N. C. Lin and John Papaloizou. "On the Tidal Interaction between Protoplanets and the
        Protoplanetary Disk. III. Orbital Migration of Protoplanets". In: *The Astrophysical Journal*
        309 (Oct. 1986), p. 846. DOI: 10.1086/164653.

[17]   D. Lynden-Bell and J.E. Pringle. "The evolution of viscous discs and the origin of the nebular
        variables." In: *MNRAS* 168 (Sept. 1974), pp. 603–637. DOI: 10.1093/mnras/168.3.603.

[18]   M. Machida et al. "Gas accretion onto a protoplanet and formation of a gas giant planet".
        In: *Monthly Notices of the Royal Astronomical Society* 405.2 (2010), pp. 1227–1243. DOI: 10.
        1111/j.1365-2966.2010.16527.x.

[19]   Alessandro Morbidelli and Sean N. Raymond. "Challenges in planet formation". In: *Journal
        of Geophysical Research: Planets* 121.10 (Oct. 2016), pp. 1962–1980. ISSN: 2169-9097. DOI:
        10.1002/2016je005088. URL: http://dx.doi.org/10.1002/2016JE005088.

[20]   NASA. *Legacy of NASA's Kepler Space Telescope: More Planets Than Stars*. URL: https:
        //www.nasa.gov/mediacast/legacy-of-nasa-s-kepler-space-telescope-more-
        planets-than-stars. (accessed: 10.02.2020).

[21]   S. -J. Paardekooper et al. "A torque formula for non-isothermal type I planetary migration -
        I. Unsaturated horseshoe drag". In: *MNRAS* 401.3 (Jan. 2010), pp. 1950–1964. DOI: 10.1111/
        j.1365-2966.2009.15782.x. arXiv: 0909.4552 [astro-ph.EP].

[22]   E. A. Petigura, A. W. Howard, and G. W. Marcy. "Prevalence of Earth-size planets orbit-
        ing Sun-like stars". In: *Proceedings of the National Academy of Sciences* 110.48 (Nov. 2013),
        pp. 19273–19278. ISSN: 1091-6490. DOI: 10.1073/pnas.1319909110. URL: http://dx.doi.
        org/10.1073/pnas.1319909110.

[23]   S Pfalzner et al. "The formation of the solar system". In: *Physica Scripta* 90.6 (Apr. 2015),
        p. 068001. ISSN: 1402-4896. DOI: 10.1088/0031-8949/90/6/068001. URL: http://dx.doi.
        org/10.1088/0031-8949/90/6/068001.

[24]   Kang-Lou Soon et al. "Investigating the gas-to-dust ratio in the protoplanetary disk of HD
        142527". In: *Publications of the Astronomical Society of Japan* (Oct. 2019). ISSN: 2053-051X.
        DOI: 10.1093/pasj/psz112. URL: http://dx.doi.org/10.1093/pasj/psz112.

[25] Moritz H. R. Stoll and Wilhelm Kley. "Vertical shear instability in accretion disc models with radiation transport". In: *Astronomy & Astrophysics* 572 (Dec. 2014), A77. ISSN: 1432-0746. DOI: `10.1051/0004-6361/201424114`. URL: `http://dx.doi.org/10.1051/0004-6361/201424114`.

[26] W. Kley et al. "Mass flow and accretion through gaps in accretion discs". In: *Monthly Notices of the Royal Astronomical Society* 303.4 (1999), pp. 696–710. DOI: `10.1046/j.1365-8711.1999.02198.x`.

[27] Ward, William R. "Planetary Accretion". In: *Completing the Inventory of the Solar System, Astronomical Society of the Pacific Conference Proceedings* 107 (1996), pp. 337–361. DOI: `1996ASPC..107..337W`.

[28] A. Wolszczan and D. A. Frail. "A planetary system around the millisecond pulsar PSR1257 + 12". In: *Nature* 355 (1992), pp. 145–147. DOI: `10.1038/355145a0`.

5.2   Abbreviations

ALMA	Atacama Large Millimeter/submillimeter Array
ESO	European Organisation for Astronomical Research in the Southern Hemisphere
VLT	Very Large Telescope

Declaration

Ich versichere, dass ich diese Arbeit selbstständig verfasst und keine anderen als die angegebenen Quellen und Hilfsmittel benutzt habe.

Heidelberg, den 14.02.2020